Organic Matter Preservation in clays from the Basal 'Hot Shale' of the Arthur Creek Formation within the Georgina Basin, Australia

Thesis submitted in accordance with the requirements of the University of Adelaide for an Honours Degree in Geology

Tom Sturman

November 2012

THE UNIVERSITY of ADELAIDE

TITLE

Organic Matter Preservation in clays from the Basal 'Hot Shale' of the Arthur Creek Formation within the Georgina Basin, Australia

ABSTRACT

Organic matter (OM) preservation in sedimentary basins has been the focus of studies since the turn of the century; however, a single unifying mechanism is yet to be accepted. Multiple hypotheses have been proposed regarding mechanisms governing OM preservation, one of which is physical protection through clay mineral adsorption. The working hypothesis for this study was that OM concentrations (total organic carbon, TOC) scale with total mineral surface area (MSA) and that without clay minerals OM is not preserved. In this study the relationship was tested with swelling clays, such as smectite, known for extremely high MSA. The observed relationship between MSA and TOC partially supports this hypothesis via a positive linear relationship between TOC and MSA, as well as the scaling of TOC to MSA when plotted against depth. Significantly however, smectite was not identified by X-ray diffraction, yet samples displayed organic carbon loadings almost double that of previous studies conducted on smectitic clays. Comparison of the MSA/TOC slope to that of measured organic carbon monolayer equivalent loading (MEL) of standards led to the conclusion the relationship is relict from depositional association which has been modified by diagenesis. Despite illitization, this relationship indicates that MSA has a significant control on OM content even after diagenesis, hydrocarbon generation, migration and degradation have occurred. It seems possible that illitization enhances the protection of OM, possibly through intragranular porosity within quartz cement. This study showed that the MSA-TOC relationship commonly observed in thermally immature modern (and some ancient) sediments extends to thermally mature illitized sediments of Mid-Cambrian age (520Ma). Evidence of biodegraded hydrocarbons, identified by GC-MS (gas chromatography-mass spectrometry), provides evidence that thermally mature clays are able to absorb migrating hydrocarbons and become associated with organic carbon in the deep burial environment.

KEYWORDS

Organic matter, Preservation, Illite, Illitization, Mineral surface area, MSA, Arthur Creek Formation, Hot Shale, Georgina Basin, Mid-Cambrian.

TABLE OF CONTENTS

Title 1
Abstract 1
Keywords 1
List of Figures and Tables 3
Introduction 4
Geological Setting 8
Materials and methods 13
Results 15
Discussion 28
Conclusion 37
Acknowledgments 38
References 39
Appendix A 43
Appendix B 55

LIST OF FIGURES AND TABLES

Figure 1: Location of sampled wells within the Southern Georgina Basin..... 6
Figure 2: Stratigraphy through Dulcie and Toko Synclines..... 9
Figure 3: Simplified cross section through sampled wells..... 12
Figure 4: MacIntyre 2 bulk XRD diffraction patterns..... 17
Figure 5: Baldwin 2 bulk XRD diffraction patterns..... 18
Figure 6: Representative clay fraction XRD diffraction patterns..... 20
Figure 7: a) Stacked slow-scan XRD diffractions patterns of representative samples
b) Enhanced view with superimposed illite polytype peaks..... 21
Figure 8: Depth relation between MSA, TOC and Carbonate for MacIntyre 2. 24
Figure 9: Depth relation between MSA, TOC and Carbonate for Baldwin 2. 25
Figure 10: Cross plot of TOC against MSA..... 26
Figure 11: Comparative cross plot of TOC against MSA 27
Figure 12: Cross plot of organic carbon loading against depth..... 31
Figure 13: Relationship of MEL to possible MSA/TOC values
a) Depositional relationship, sample TOC scales with MSA on with a 1:1 relationship
b) Diagenetic relationship; MSA loss from illitization without hydrocarbon migration
c) Diagenetic relationship; MSA loss from illitization and hydrocarbon generation
d) Diagenetic relationship; MSA and relative TOC loss from addition of material 32

Table I: Qualitative bulk sample mineralogy.....16
Table II: Clay fraction mineralogy.....19
Table III: Summarised TOC and MSA data.....22

INTRODUCTION

Preservation of organic matter (OM) has been the focus of studies dating back to the turn of the century (Schuchert 1915). Rising energy consumption over recent years (5.6% p.a. globally) (Jing *et al.* 2011) has seen interest in this area grow substantially over the past few decades, as the oil and gas industry turn to unconventional reservoirs as a viable hydrocarbon source. Understanding how OM is preserved over geological timescales will allow for improved predictions of hydrocarbon distribution in sedimentary basins, greatly aiding exploration and production. The previous assumption of shale homogeneity has proved problematic with significant production variability observed in well-developed hydrocarbon fields in the U.S. (Bustin *et al.* 2008). This production variability is yet to be adequately explained, however may be related to OM distribution within shales caused by varying levels of preservation, dilution and deposition of OM.

A variety of mechanistic theories have been proposed, explaining how preservation of OM occurs on geological time scales. Some studies have suggested that preservation is a consequence of sediment and bottom-water anoxia (Demaison and Moore 1980), rates of OM production versus deposition (Tyson 2001; Bohacs *et al.* 2005) and rates of sedimentation and the resulting OM dilution (Coleman *et al.* 1979; Katz 2005). Other studies have focused on the physical protection offered by sediments, for example Lünsdorf *et al.* (2000) proposed that 'clay hutch' structures were able to physically protect OM from degradation. Studies conducted on modern sediments (and some ancient) from various depositional settings identified correlations between organic carbon content and decreasing sediment mineral size (increasing mineral surface area),

suggesting that OM is physically protected by mineral surfaces which facilitates preservation (Suess 1973; Tanoue and Handa 1979; Mayer *et al.* 1985; Keil and Hedges 1993; Mayer 1994; Keil *et al.* 1994 A; Keil *et al.* 1994 B; Bergamashi *et al.* 1997; Ransom *et al.* 1998; Kennedy *et al.* 2002; Kennedy and Wagner 2011).

An important step forward in understanding OM preservation is the proposal by Mayer (1994) that OM forms and is preserved as a single molecular mono-layer coating on minerals surfaces. Although Ransom *et al.* (1997) argued against this theory, based on transmission electron microscopy (TEM) images showing sporadic coverings of OM rather than continuous coatings on the mineral surfaces, subsequent studies have documented in a variety of settings that OM coverings are commonly equivalent to a monolayer coating (Hedges and Keil 1995; Ransom *et al.* 1998; Curry *et al.* 2007; Kennedy 2011). Recently this relationship, between mineral size and OM content, has also been observed in ancient sediments (<100Ma) which have undergone modest burial; though burial depth was insufficient to influence mineralogy or organic carbon maturation and hydrocarbon generation (Kennedy *et al.* 2002; Kennedy and Wagner 2011).

The current study follows the relation between MSA and OM previously established in thermally immature modern and Cretaceous sediments into deeply buried sediments, typically found in gas producing successions. It tests if a hypothesized preservative effect of total mineral surface area (MSA) is able to explain variations in organic carbon enrichment (total organic carbon percent, TOC) within much older and thermally mature Mid-Cambrian sediments. The study was conducted using samples from the

Basal 'Hot Shale' of the Arthur Creek Formation in the Southern Georgina Basin, Northern Territory Australia (Figure 1). This formation was chosen because of its age as well as high and variable TOC content within the shale sub-unit, documented as high as 16% (Pegum 1997; Ambrose and Putnam 2005B). Mid- to Late-Cambrian sedimentary successions within the Georgina Basin (such as the Arthur Creek Formation) are also known to host prospective oil stains throughout (Boreham and Ambrose 2007); should any significant relationships be identified, it will have significant implications for production from prospective unconventional systems in the region.

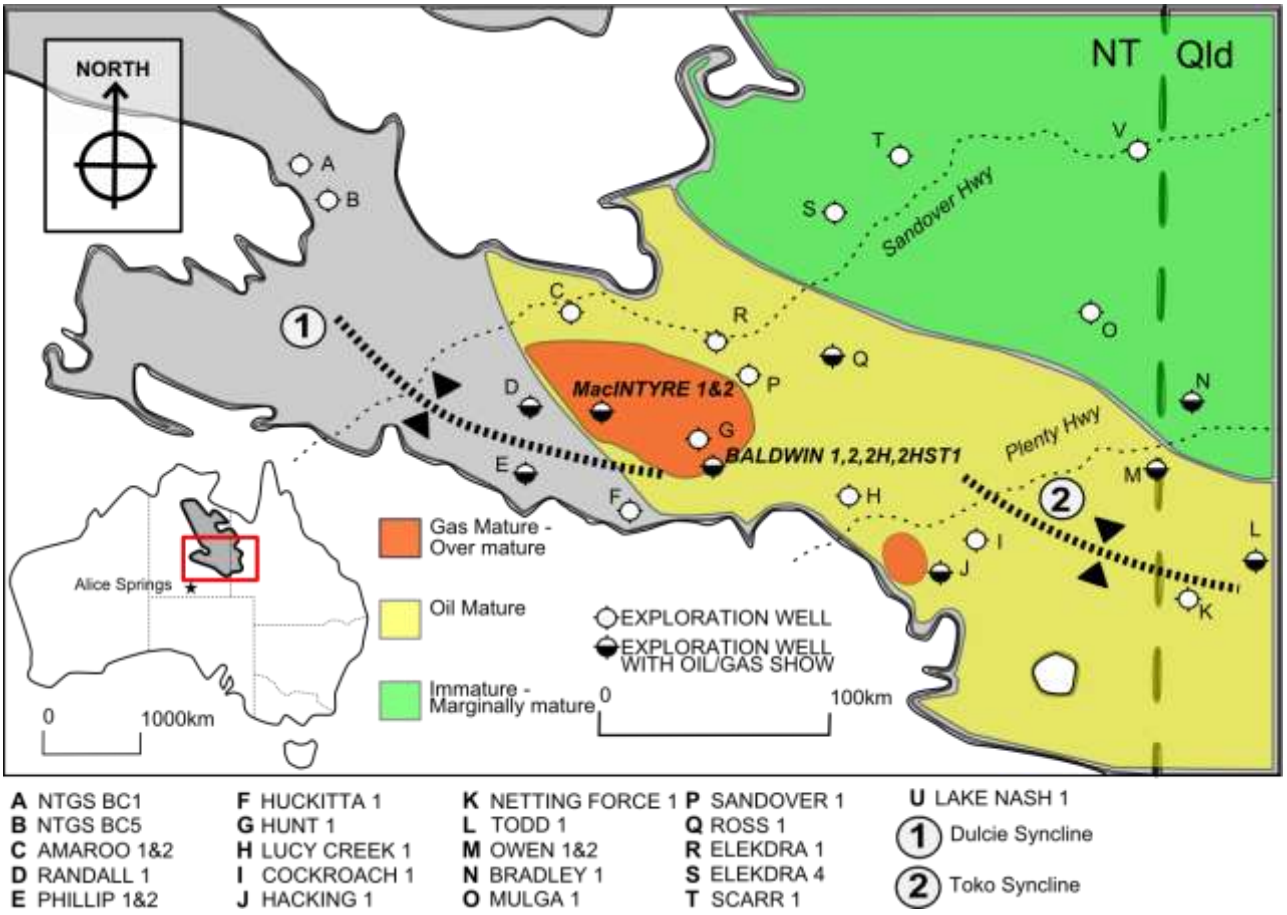

Figure 1: Location of sampled wells within the Southern Georgina Basin (MacIntyre 2 and Baldwin 2) with superimposed source maturation distribution for Lower Arthur Creek formation as well as Dulcie and Toko Synclines. Additional exploration wells with corresponding hydrocarbon shows are represented as A-U. Figure modified from Ambrose *et al.* (2001) and Boreham and Ambrose (2007).

18°S

The conventional model explaining OM distribution in sedimentary rocks describes micron-scale organic particles deriving from phytoplankton, deposited as discrete grains within sediment. This style of deposition causes OM to be physically independent to the mineral phases with which it is deposited, and therefore does not scale to any mineralogical properties (e.g. MSA). With this model, any alteration of the OM during burial or diagenesis is independent from the mineralogy of surrounding sediments.

The working hypothesis of this study is that clay minerals present a first order control on the OM which survives initial burial, causing OM to scale with MSA, and that this proportionality is retained after burial diagenesis. To test this, the TOC of well cuttings from thermally mature sediments will be compared to sample MSA determined by the modified Ethylene Glycol Monomethyl Ether (EGME) method of Cihacek & Bremner (1979). A positive MSA/TOC correlation and scaling of TOC to MSA against depth would support the hypothesized preservative effect of MSA. If a relationship cannot be identified the hypothesis will be falsified, or, any relationship established in the depositional environment will be assumed to have been lost through diagenesis.

GEOLOGICAL SETTING

The Georgina Basin is the largest Neoproterozoic-Palaeozoic (1000Ma – 250Ma) intracratonic basin on the North Australian craton (Figure 1). The basin is an erosional relic of a series of originally connected intracratonic basins, and currently covers over 330,000 km^2 (Dunster *et al.* 2007). The basin displays a north-west trend (Smith 1972) with a latitudinal span from 25˚S to 18˚S (Smith 1972; Dunster *et al.* 2007), stretching across the Northern Territory and Queensland border (Figure 1). Carbonate and clastic sediments are preserved within the Georgina Basin, ranging in ages from Cambrian to Ordovician in the north (Pegum 1997) and Neoproterozoic to Devonian in the south (Ambrose and Putnam 2005A). Ambrose *et al.* (2001) defines the basin's current margins as frequently faulted unconformities; bound to the north, south, east and west respectively by the Proterozoic McArthur and South Nicholson Basins, the Arunta Block, the Mt. Isa Block, and the Tennant Creek and Arunta Blocks.

The Georgina Basin was originally part of a much larger Neoproterozoic succession, contiguous with what are currently known as the Amadeus, Ngalia and Officer Basins (Hill and Walter 2000; Dunster *et al.* 2007), as well as (possibly) the Wolfe and Birrindudu Basins (Lindsay 2002). By the Late-Ediacaran (550Ma), major plate reconstruction was underway corresponding to the Petermann Orogeny, which caused a rift system to develop and the Georgina Basin to separate from the larger Neoproterozoic succession. Prior to the separation of the aforementioned basins the Plenty, Aroota, Keepera and Mopunga Groups were respectively deposited (Figure 2) (Dunster *et al.* 2007). These groups record fluvial silicilastic, glacial, intertidal and shallow marine depositional environments (Dunster *et al.* 2007).

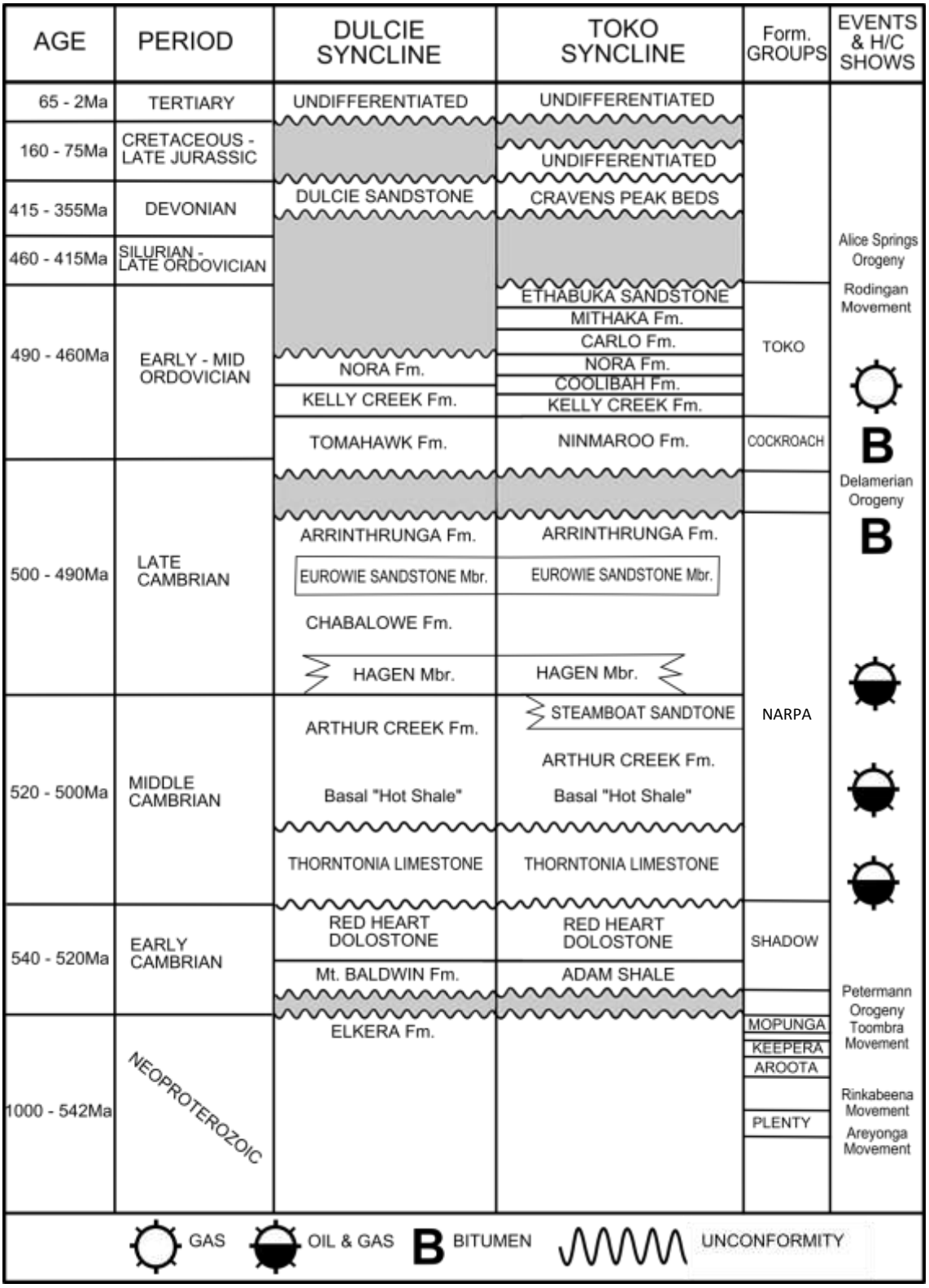

Figure 2: Stratigraphy through Dulcie and Toko Synclines, Southern Georgina Basin. Tectonic events and hydrocarbon occurrences are shown adjacent. Figure modified from Ambrose and Putnam (2005A; 2005B), Boreham and Ambrose (2007) and Dunster *et al.* (2007).

Following the Petermann Orogeny (550-535Ma), the basin experienced tectonically stable conditions and a carbonate platform was deposited (Red Heart Dolostone), marking the top of the Shadow Group (Figure 2) (Dunster *et al.* 2007). The Shadow Group records an Early- to Mid-Cambrian sedimentary succession, deposited in a foreland-sag setting in the southern portion of the basin. The Mid- and Late-Cambrian Narpa and Cockroach Groups were deposited above the carbonate platform (Dunster *et al.* 2007). The Narpa Group represents a basin wide shoaling upward sequence (Ambrose and Putnam 2005A) and hosts conventional and unconventional hydrocarbon targets, including the Thorntonia Limestone and Basal 'Hot Shale' of the Arthur Creek Formation (Figure 2). Deposition of the Narpa and Cockroach Groups was interrupted by the Delamerian Orogeny (515-500Ma), causing localized relative uplift (Dunster *et al.* 2007). The 'Hot Shale' is a condensed transgressive deposit (Ambrose and Putnam 2005A) occurring in the southern portion of the basin, likely deposited in an outer shelf/slope environment, based on Bathynotus trilobite fossils identified at the base of the formation (Shergold and Whittington 2000). The remaining Arthur Creek Formation represents highstand deposits (Ambrose and Putnam 2005A).

Synsedimentary normal faulting caused by extensional rifting affected deposition of marine siciliclastic sediments during Early-Ordovician (487Ma). By the Late-Ordovician (445Ma), subduction along Australia's eastern margin terminated all extension (Dunster *et al.* 2007). The Alice Springs Orogeny (450-300Ma) reactivated northwest trending structures in a reverse sense, and was the most severe deformational event to affect the basin (Dunster *et al.* 2007). The most prominent structural features within the Southern Georgina Basin are the Dulcie and Toko Synclines, respectively

preserving up to 3.7km and 1.5km of sediment. Smith (1972) comments that despite the tectonic activity which effected the basin, sediments remain unmetamorphosed.

Ambrose and Putnam (2005B) suggest the most prospective formations of the Georgina Basin are the (conventional) Thorntonia Limestone and the (unconventional) Arthur Creek Formation; the Arthur Creek Formation unconformably overlies the Thorntonia Limestone in the southern portion of the basin. These plays are localized in and around the Dulcie and Toko Synclines and remain largely unexplored, with only 1 well per 6000km^2 (Ambrose *et al.* 2001; Ambrose and Putnam 2005A). Agnostine trilobite fossils have been used to date the Arthur Creek Formation as a whole (Mid-Cambrian, 520Ma), while the thickness is known to reach over 650m (Dunster *et al.* 2007). MacIntyre 2 intersects the Arthur Creek Formation with a thicknesses of approximately 300m, expanding in an east-south-easterly direction to 415m in Baldwin 2 (Figure 3); thicknesses interpreted from wireline logs and well cuttings.

The Basal 'Hot Shale' was interpreted by Ambrose and Putnam (2005A) as deposited during a marine transgression, resulting in low energy dolomitic sands/silts, dolomite, and shale deposited under anoxic conditions. The TOC of the 'Hot Shale' is known to reach up to 16% (Pegum 1997; Ambrose and Putnam 2005A). The upper portion of the Arthur Creek Formation was deposited during regression, consisting predominantly of carbonate sediments with superimposed upward shoaling cycles (Ambrose and Putnam 2005A). The sand content of the formation is interpreted to increase northwards, based on the lithology in Mulga-1 (Ambrose and Putnam 2005A). High temperature basement granites at the southern margin of the Georgina Basin causing the Arthur Creek

Formation to grade from immature in the north, to gas- and over-mature in the south (Figure 1) (Ambrose and Putnam 2005A). Referring specifically to the maturity of the wells sampled for this study (Figure 1); MacIntyre 2 falls within an area considered to be gas-over mature, while Baldwin 2 lies on the boundary between oil mature and gas-over mature (Boreham and Ambrose 2007).

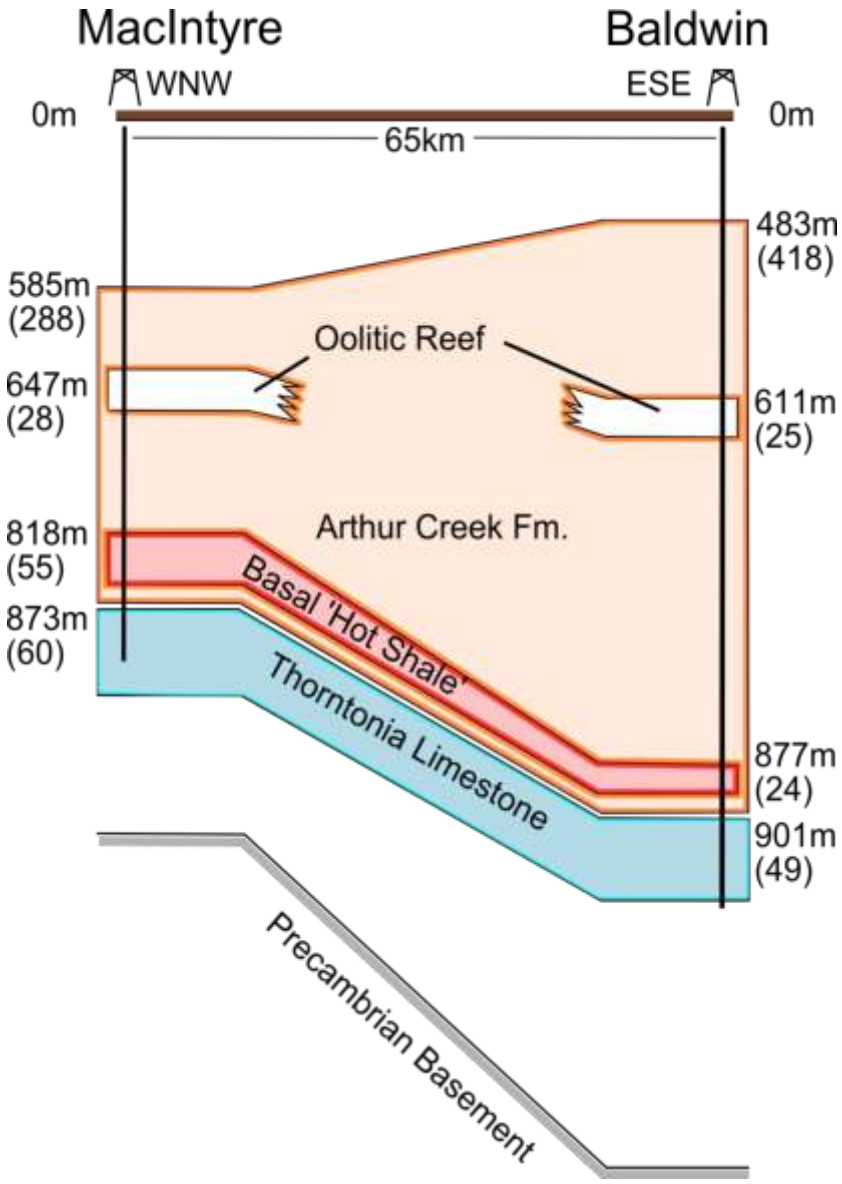

Figure 3: Simplified cross section through sampled wells, MacIntyre 2 and Baldwin 2. Formation depths and correlations based on wireline data and lithological analysis on well cuttings, as concluded by PetroFrontier Corp., thicknesses displayed in brackets. Cross section is intended only as an aid for visualizing formation depth and thickness variations between wells. Illustrated depths and thicknesses are not to scale.

MATERIALS AND METHODS

The current study utilized 25 cutting samples collected from two wells penetrating the Basal 'Hot Shale' of the Arthur Creek Formation in the Southern Georgina Basin. Samples were collected from MacIntyre 2 and Baldwin 2 (Figures 1 & 3), and were selected based on high/low shale content as identified on gamma wireline logs so as to capture a variability in grain size. Samples and wireline logs were provided by PetroFrontier Corp. Due to sampling restrictions; sample resolution was limited to meter-scale. Prior to analysis, all samples were dried for ≥24hrs at 40˚C and ground using an agate mortar then passed through a 250µm sieve. The location of sampled wells, MacIntyre 2 and Baldwin 2, are illustrated in Figure 1, while depth and thickness variations in the Arthur Creek Formation and Thorntonia Limestone between wells are expressed in Figure 3.

Mineralogy was determined from randomly orientated bulk powder samples, using X-ray diffraction (XRD; Bruker D8 Advance XRD with Cu source). Samples were scanned between 3.5˚ - 50˚2θ using a 0.02˚ step size and 1s dwell time. Mineral phases were identified in the Diffrac.Eva software package using reference patterns from the Open Crystallography Database. Clay mineralogy was determined on orientated preparations of the <5µm fraction and prepared as per Moore and Reynolds (1996). Clay fractions were scanned for 20 minutes between 3.5˚ - 45˚2θ using a 0.003˚ step size.

Sample TOC was calculated by subtracting the inorganic carbon content, determined using a modified version of the pressure calcimeter method of Sherrod *et al.* (2002),

from the total carbon content, identified using a Carbon-Hydrogen-Nitrogen analyser (LECO TruSpec CHN). MSA was determined with EGME, using the 'free surface' procedure of Cihacek and Bremner (1979). EGME was chosen over the more common N_2-BET adsorption method because unlike N_2-BET it permits measurement of total MSA (internal and external mineral surfaces) within expandable clay minerals. Clay mineral standards were run simultaneously to test the accuracy and precision of the EGME-MSA results; standards were acquired from the Clay Mineral Society as well as 'in-house' field sampling. The standards run were Ca-rich Montmorillonite (STx-1b, Clay Min. Society), Na-rich Montmorillonite (SWy-2, Clay Min. Society), Mancos Smectite (M.Std, in-house), Mancos weathered Smectite (M.Wth, in-house) and a Cambrian shale Illite (IMt-2, Clay Min. Society). Standards respectively returned relative standard errors of 1.27%, 0.37%, 2.74%, 2.64% and 6.34%.

Gas chromatography-mass spectrometry (GC-MS) was conducted using micro-scale sealed vessels (MSSV) to characterise OM present within the samples. GC-MS was run on 4 samples per well, selected to represent TOC variability with depth. Analysis was undertaken using a Quantum MSSV injector fitted to a Hewlett Packard 6890/5973 GC-MS system and was analysed under standard parameters, see Hall *et al.* (1999) and Hall *et al.* (2011). For a full, detailed methodology, see Appendix A.

RESULTS

XRD analysis of bulk samples indicates that despite meter-scale sampling resolution, and total vertical separation of 87m, all samples have a relatively consistent mineralogy (Table I, Figures 4 & 5). Analysis of orientated clay fraction preparations revealed both detrital and diagenetic illite within the clay fraction (Figures 6 & 7). Differentiation between detrital and diagenetic illite was based on diagnostic reflection peaks for illite polytypes (Moore and Reynolds 1996) using slow-scan XRD on bulk powdered samples (12s dwell time, 0.02˚ step size, 3.5˚2θ-50˚2θ), illustrated in Figure 7. Notably neither smectite nor mixed layer illite/smectite were identified (Table II).

TOC and MSA presented herein are on a carbonate free basis, corrected for to account for the presence of any carbonate cement. Carbonate has no significant surface area and can cause an inaccurate correlation between MSA and TOC through dilution of OM. To focus on the association of OM to the clay mineral phase, carbonate percent has been subtracted from MSA and TOC values. Raw data presented in Appendix B.

Calculating TOC identifies the siliciclastic phase of MacIntyre 2 reaching up to 8.54% (average 4.24%) and Baldwin 2 up to 9.20% (average 4.70%), summarized in Table III. Noticeably, samples from MacIntyre 2 display increasing TOC with depth. A similar increase is observed for Baldwin 2 samples with a prominent oscillation. Despite their differences, both wells reach peak TOC at the base of the 'Hot Shale', as shown in Figures 8 & 9, (MacIntyre 2 sample 894 excluded here due anonymously high carbonate content, 95%, and the introduced error to MSA and TOC measurement).

Table I: Qualitative bulk sample mineralogy with interpretations based on XRD of bulk powdered sample; composition is that of typical shale (Shaw and Weaver 1965). Analysis conducted using Bruker D8 XRD with Cu source, run between 3.5°2θ and 50°2θ with 0.02° step size and 1s dwell time. Note, bulk XRD identified biotite within the clay fraction, this was later revised to illite based on analysis of the <5µm fraction. Mineral phases interpreted with Diffrac.Eva software package using reference patterns from the Open Crystallography Database. For representative XRD diffraction patterns, refer to Figures 4 & 5.

Sample	*Qz.*	*Cal.*	*Dol.*	*Flr.*	*Pyr.*	*Mus.*	*Alb.*	*Ill.*	*Fld.*	*Chl.*
B2.873	X	X	X	X	X	X				
B2.876	X	X	X				X	X		X
B2.879	X	X	X	X	X		X	X		
B2.881	X	X	X	X	X		X	X		X
B2.883	X	X	X	X			X	X	X	X
B2.886	X	X	X	X			X	X		X
B2.888	---	---	--- INSUFFICIENT SAMPLE FOR ANALYSIS ---						---	---
B2.890	X	X	X	X	X		X	X		X
B2.893	X	X	X	X	X	X	X	X		X
B2.894	X	X	X	X	X		X	X		X
B2.897	X	X	X	X	X		X	X		X
B2.900	X	X	X	X	X		X	X	X	X
B2.903	X	X	X	X	X			X		X
B2.906	X	X	X	X	X		X	X		
M2.819	X	X	X	X	X		X			X
M2.828	X	X	X	X	X		X			X
M2.837	X	X	X	X	X		X	X		X
M2.843	X	X	X	X	X		X	X		X
M2.852	X	X		X			X			
M2.858	X	X		X	X		X	X		X
M2.861	X	X		X	X		X	X		X
M2.870	X	X	X	X	X		X	X		X
M2.876	X	X	X	X			X			
M2.879	X	X	X	X			X			
M2.890	X	X	X	X			X			

Qz.= Quartz	Flr.=Fluorapatite	Alb.= Albite	Chl.= Chlorite
Cal.= Calcite	Pyr.= Pyrite	Ill.= Illite	
Dol.= Dolomite	Mus.= Muscovite	Fld.= Feldspar	X = mineral presence interpreted

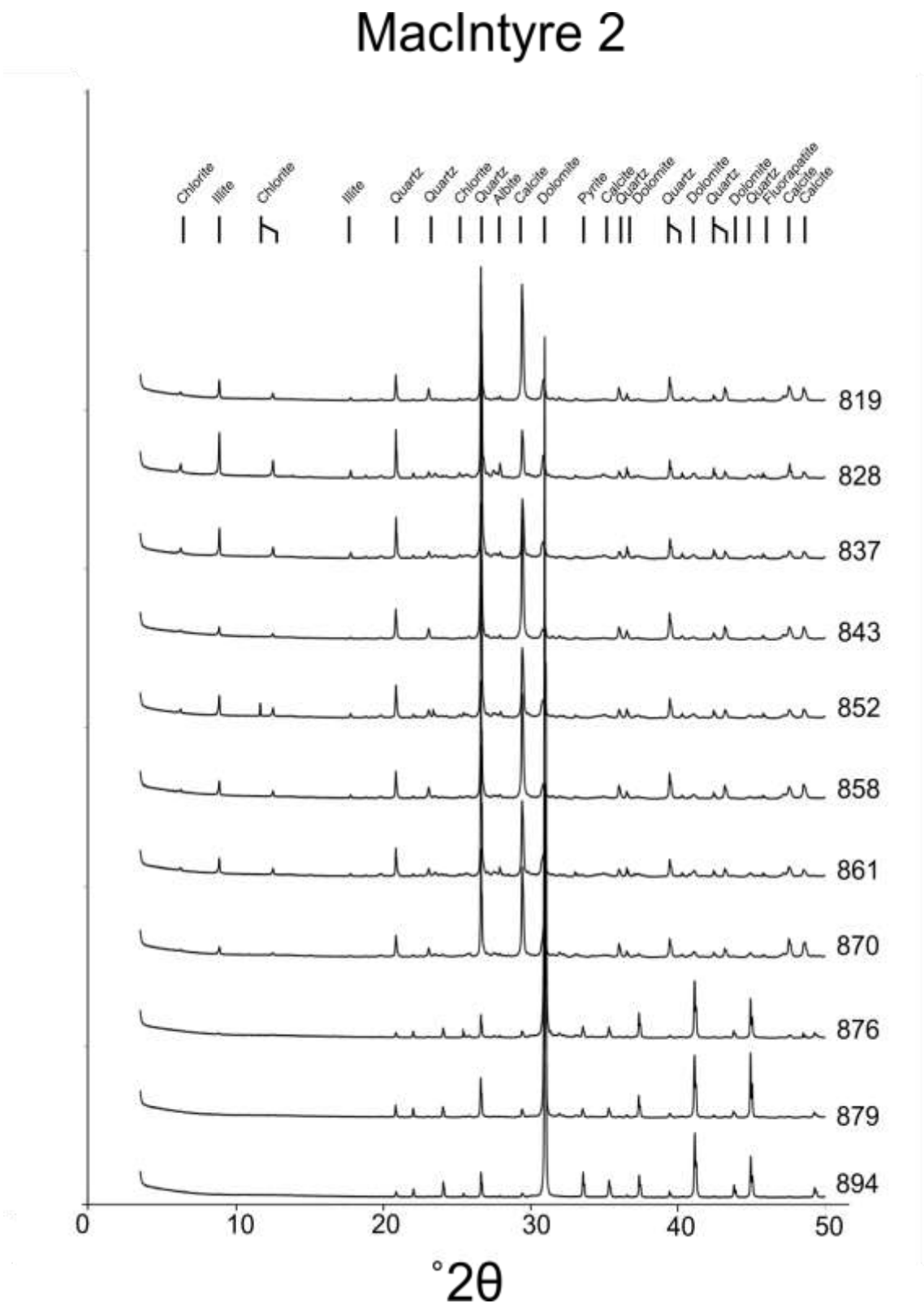

Figure 4: MacIntyre 2 bulk XRD diffraction patterns stacked with depth and superimposed diagnostic peak positions. Vertical axis scaled to facilitate pattern stacking and illustrate peak variability. Analysis conducted on powdered samples using a Bruker D8 Advance XRD with Cu source. Samples were scanned between 3.5˚-50˚2θ using a 0.02˚ step size and 1s dwell time. Note, bulk XRD identified biotite within the clay fraction, this was later revised to illite based on analysis of the <5µm fraction. Mineral phases interpreted with Diffrac.Eva software package using reference patterns from the Open Crystallography Database.

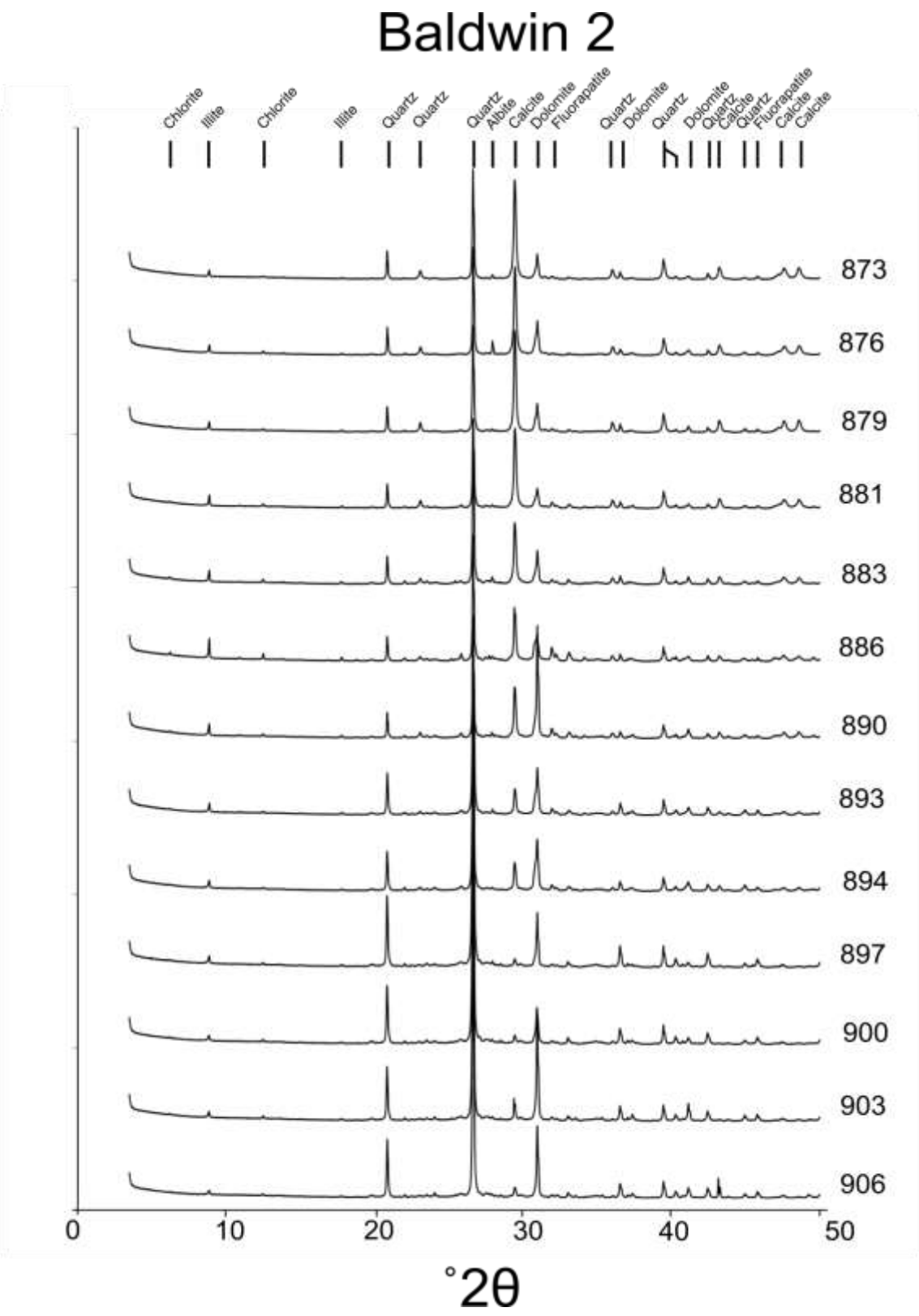

Figure 5: Baldwin 2 bulk XRD diffraction patterns stacked with depth and superimposed diagnostic peak positions. Vertical axis scaled to facilitate pattern stacking and illustrate peak variability. Analysis conducted on powdered samples using a Bruker D8 Advance XRD with Cu source. Samples were scanned between 3.5˚-50˚2θ using a 0.02˚ step size and 1s dwell time. Note, bulk XRD identified biotite within the clay fraction, this was later revised to illite based on analysis of the <5µm fraction. Mineral phases interpreted with Diffrac.Eva software package using reference patterns from the Open Crystallography Database.

Table II: Clay fraction mineralogy interpreted from clay fraction thin film XRD and changes in interlayer spacing after exposure to varied conditions; air-dried, EG-wet, 400˚C and 550˚C. Analysis conducted using Bruker D8 XRD with Cu source, run for total duration of 20 minutes between 3.5˚2θ and 45˚2θ with 0.003˚ step size. Interpretations based on interlayer spacing responses to varied exposures as per Clay Mineral Identification Flow diagram from U.S. Geological Survey Open-File Report 01-041 (U. S. Geological Survey 2011). For representative XRD diffraction patterns, refer to Figure 6.

Sample	*Interlayer spacing (Å)*	*Interpreted mineralogy*
B2.879	14	Chlorite
	10	Illite
	7	Chlorite
B2.900	14	Chlorite
	10	Illite
	7	Chlorite
M2.819	14	Chlorite
	10	Illite
	7	Chlorite
M2.828	14	Chlorite
	10	Illite
	7	Chlorite
M2.837	14	Chlorite
	10	Illite
	7	Chlorite
M2.843	14	Chlorite
	10	Illite
	7	Chlorite
M2.852	14	Chlorite
	10	Illite
	7	Chlorite
M2.858	14	Chlorite
	10	Illite
	7	Chlorite
M2.861	14	Chlorite
	10	Illite
	7	Chlorite
M2.870	14	Chlorite
	10	Illite
	7	Chlorite

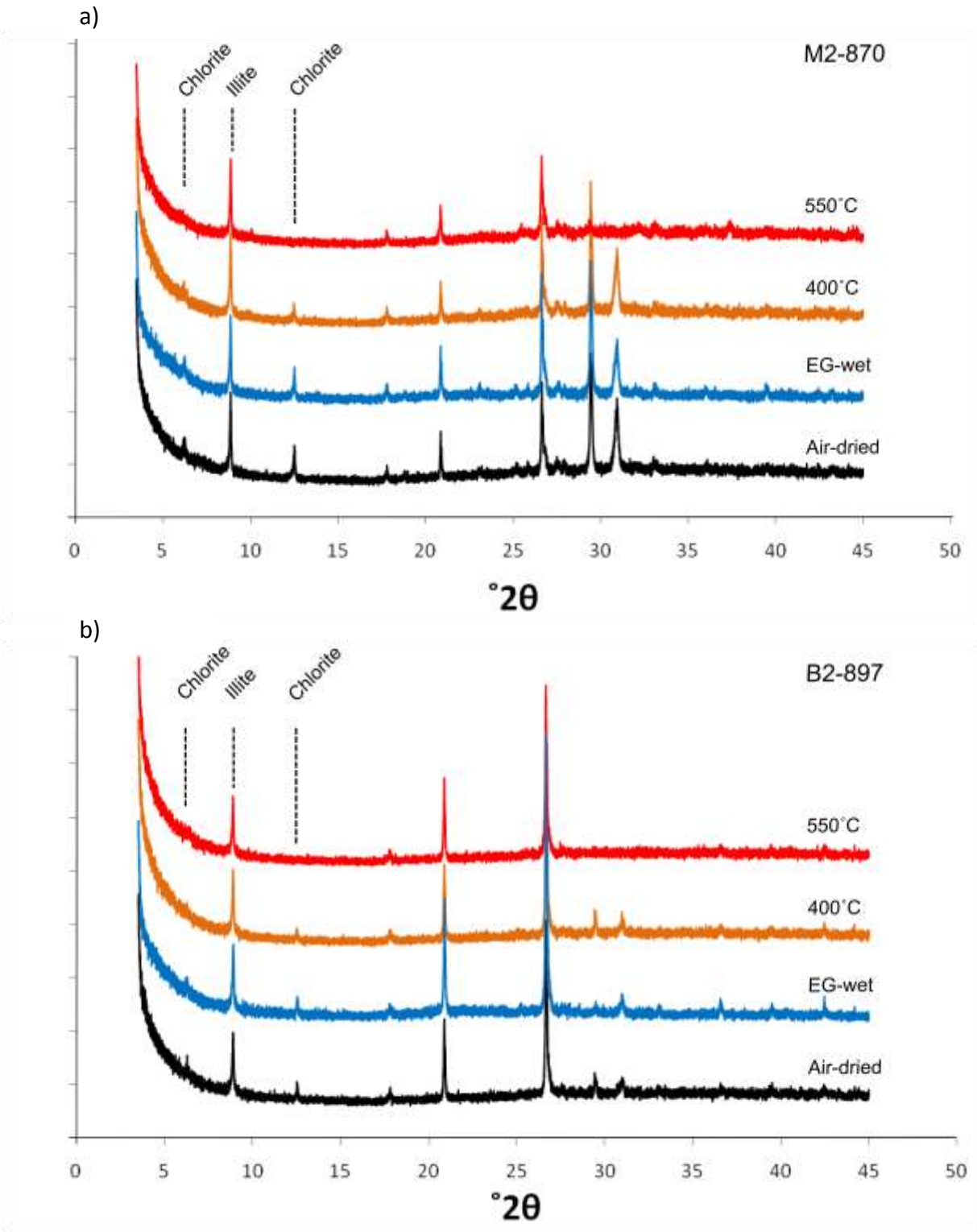

Figure 6: Representative clay fraction XRD diffraction patterns displaying air-dried (black), EG-wet (blue), 400˚C (orange) and 550˚C (red) exposures for a) MacIntyre 2 and b) Baldwin 2. Interpretations based on interlayer spacing response to varied exposures as per Clay Mineral Identification Flow diagram from U.S. Geological Survey Open-File Report 01-041 (U. S. Geological Survey 2011). Analysis conducted on <5µm samples using a Bruker D8 Advance XRD with Cu source. Samples were scanned between 3.5˚-45˚2θ using a 0.003˚ step size, total duration of 20 minutes per sample.

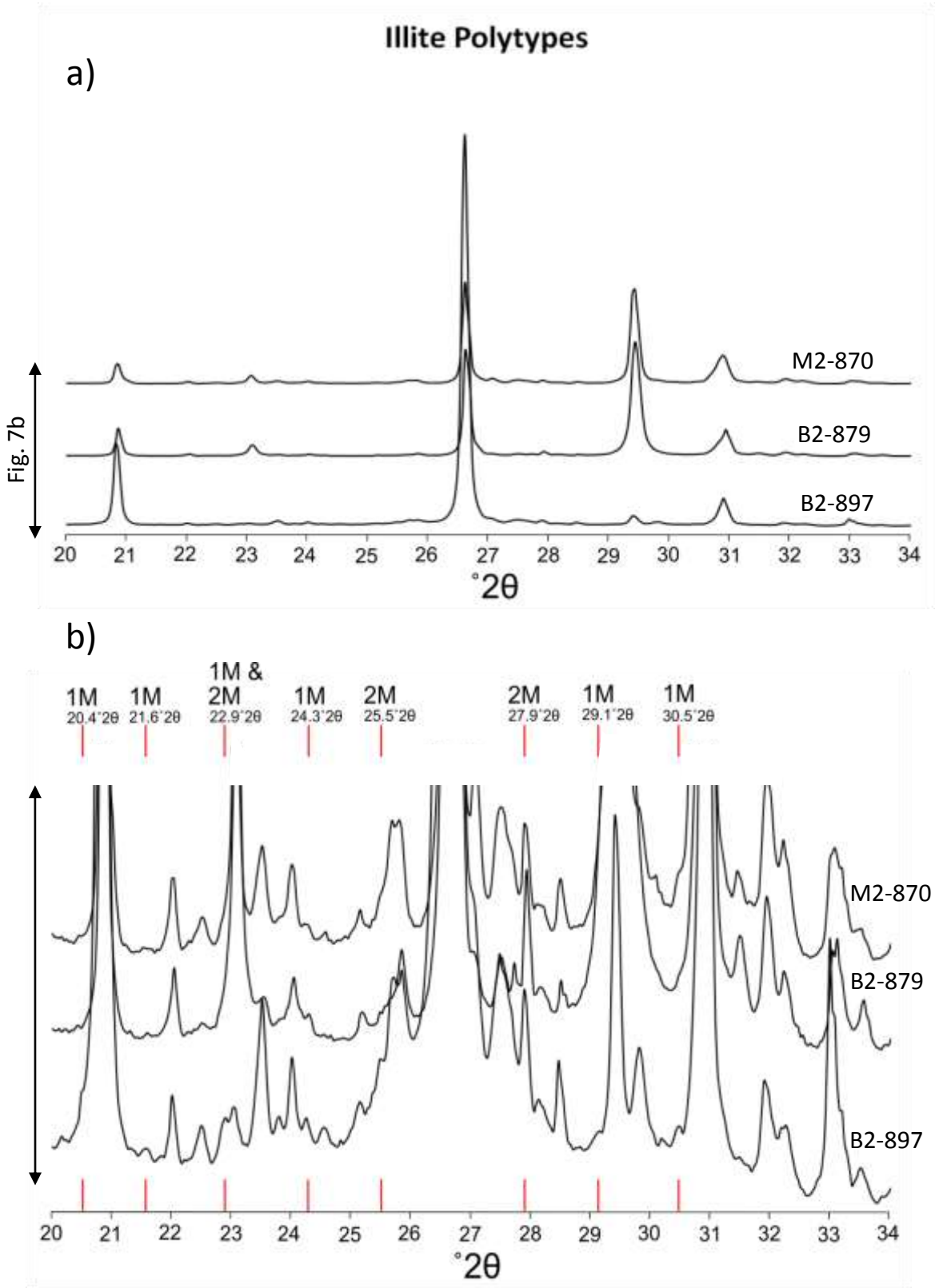

Figure 7: a) Stacked slow-scan XRD diffractions patterns of representative samples. b) Enhanced view with superimposed illite polytype peaks illustrating presence of diagenetic (1M) and detrital (2M) illite; scaled vertical axis to facilitate peak identification. Polytype peaks identified based on Moore and Reynolds (1996). Samples chosen based on bulk powder XRD appearing representative of relative sample sets. Analysis conducted on powdered samples using a Bruker D8 Advance XRD with Cu source. Samples were scanned between 3.5˚-50˚2θ using a 0.02˚ step size and 12s dwell time.

Table III: Summarised TOC and MSA data, pre- and post- carbonate correction. TOC determined by subtracting the inorganic carbon content from total organic carbon content. MSA calculated using free surface area method of Tiller & Smith (1990). TOC values were carbonate corrected, MSA values were corrected for carbonate and TOC content. Corrected values are used to account for the variable effect of carbonate dilution.

Sample	*$CaCO_3$ (%)*	*TOC (%)*		*MSA (m^2/g)*	
		Raw	*Corrected	Raw	**Corrected
B2.873	62.19	0.75	2.00	17.70	47.76
B2.876	60.07	0.12	0.30	22.52	56.57
B2.879	60.24	1.15	2.90	22.88	59.28
B2.881	64.12	0.21	0.58	27.92	78.28
B2.883	45.95	1.74	3.22	30.19	57.71
B2.886	38.65	1.54	2.51	24.26	40.57
B2.888	54.72	1.67	3.70	23.09	52.96
B2.890	49.93	1.06	2.12	25.56	52.16
B2.893	33.78	4.78	7.22	61.65	100.35
B2.894	36.71	5.52	8.72	59.82	103.56
B2.897	11.13	8.17	9.20	62.78	77.79
B2.900	15.54	6.60	7.82	56.29	72.30
B2.903	38.72	4.30	7.01	52.17	91.54
B2.906	23.18	6.53	8.50	52.21	74.28
M2.819	56.41	0.59	1.35	12.19	28.36
M2.828	35.30	0.64	0.99	13.82	21.58
M2.837	37.34	1.06	1.69	20.39	33.11
M2.843	51.36	1.34	2.75	14.93	31.57
M2.852	42.41	1.89	3.28	20.22	36.29
M2.858	54.15	2.05	4.48	19.43	44.36
M2.861	45.70	2.60	4.78	25.30	48.94
M2.870	53.58	3.33	7.17	27.05	62.75
M2.876	88.81	0.96	8.54	9.20	89.91
M2.879	78.78	1.56	7.38	10.20	51.89
M2.894	94.53	0.87	15.88	5.49	119.27

** $CaCO_3$ corrected ** $CaCO_3$ & TOC corrected*

Comparing MSA values for each well against depth identified trends similar to that of TOC (Figures 8 & 9). MSA within MacIntyre 2 increases steadily with depth, while Baldwin 2 displays MSA increasing with depth in an oscillating manner. TOC displays similar trends within respective wells. Notably, MacIntyre 2 displays the most prominent scaling of TOC to MSA, the association becoming tighter with depth.

Cross plotting TOC against MSA identifies a positive relationship between the variables in both wells (Figures 10 & 11). MacIntyre 2 and Baldwin 2 each display different slopes, likely corresponding to different depositional or preservational settings. MacIntyre 2 samples exhibit a much stronger correlation than samples from Baldwin 2 with correlation coefficients respectively of $R^2 = 0.94$ and $R^2 = 0.48$. Notably however, samples from Baldwin 2 appear to be divided into two clusters of high and low TOC, skewing their correlation.

In a similar study conducted by Kennedy *et al.* (2002) and Kennedy & Wagner (2011) it was shown that MSA is similar in samples with OM removed through chemical oxidation and in untreated samples. A slight increase in MSA was identified in samples with OM removed, attributed to the opening of pore spaces. This observation demonstrates that EGME does not interact with OM within the sample, validating the correlation between MSA and TOC observed here.

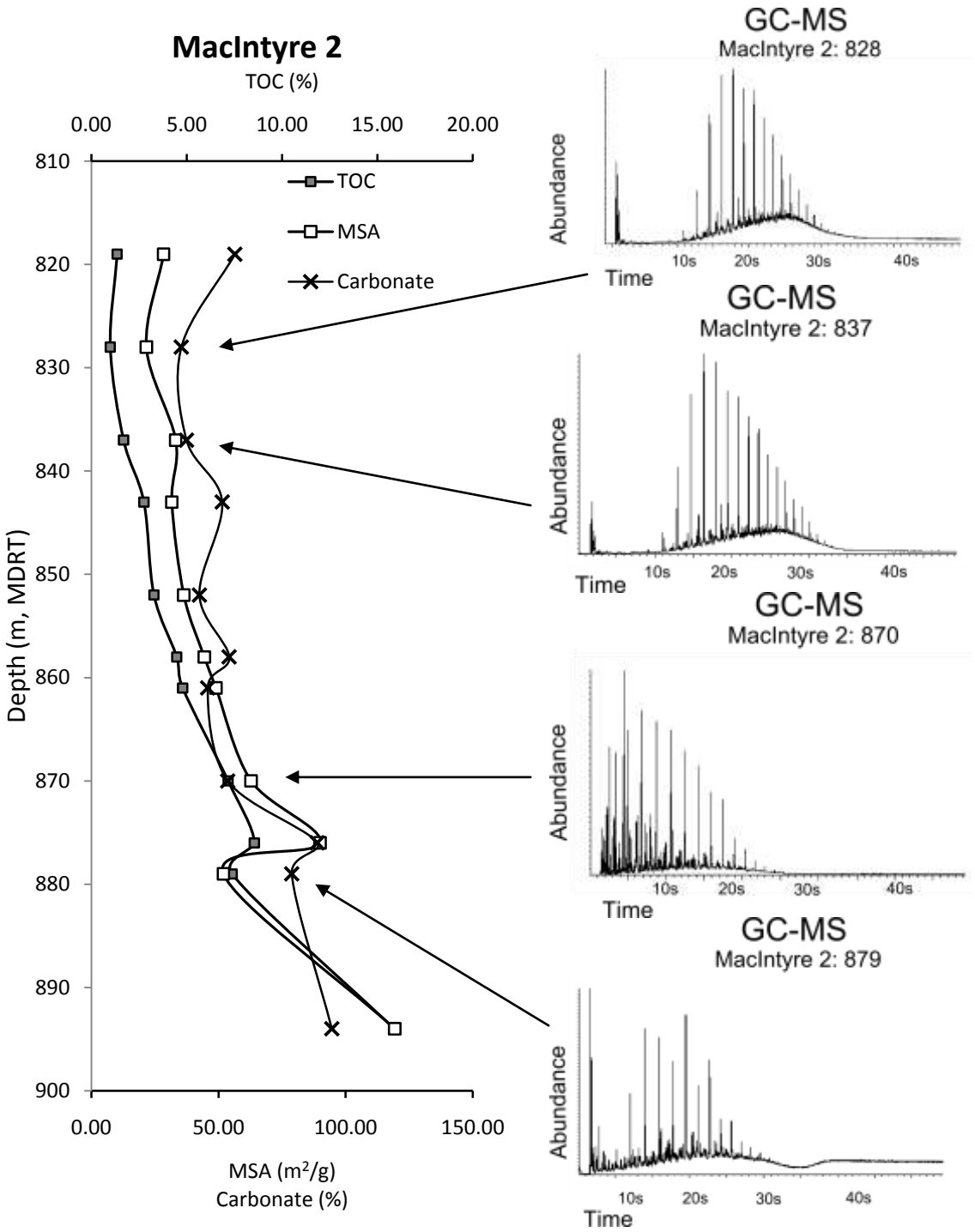

Figure 8: Depth relation between MSA, TOC and Carbonate for MacIntyre 2. MSA and TOC values used were corrected for carbonate content through subtraction. GC-MS hydrocarbon profiles are shown adjacent to depth plots. Clay Mineral Society and in-house clay standards we run simultaneously; STx-1b, SWy-2, M.Std, M.Wth, and IMt-2. Standards returned relative standard errors of 1.27%, 0.37%, 2.74%, 2.64% and 6.34% respectively.

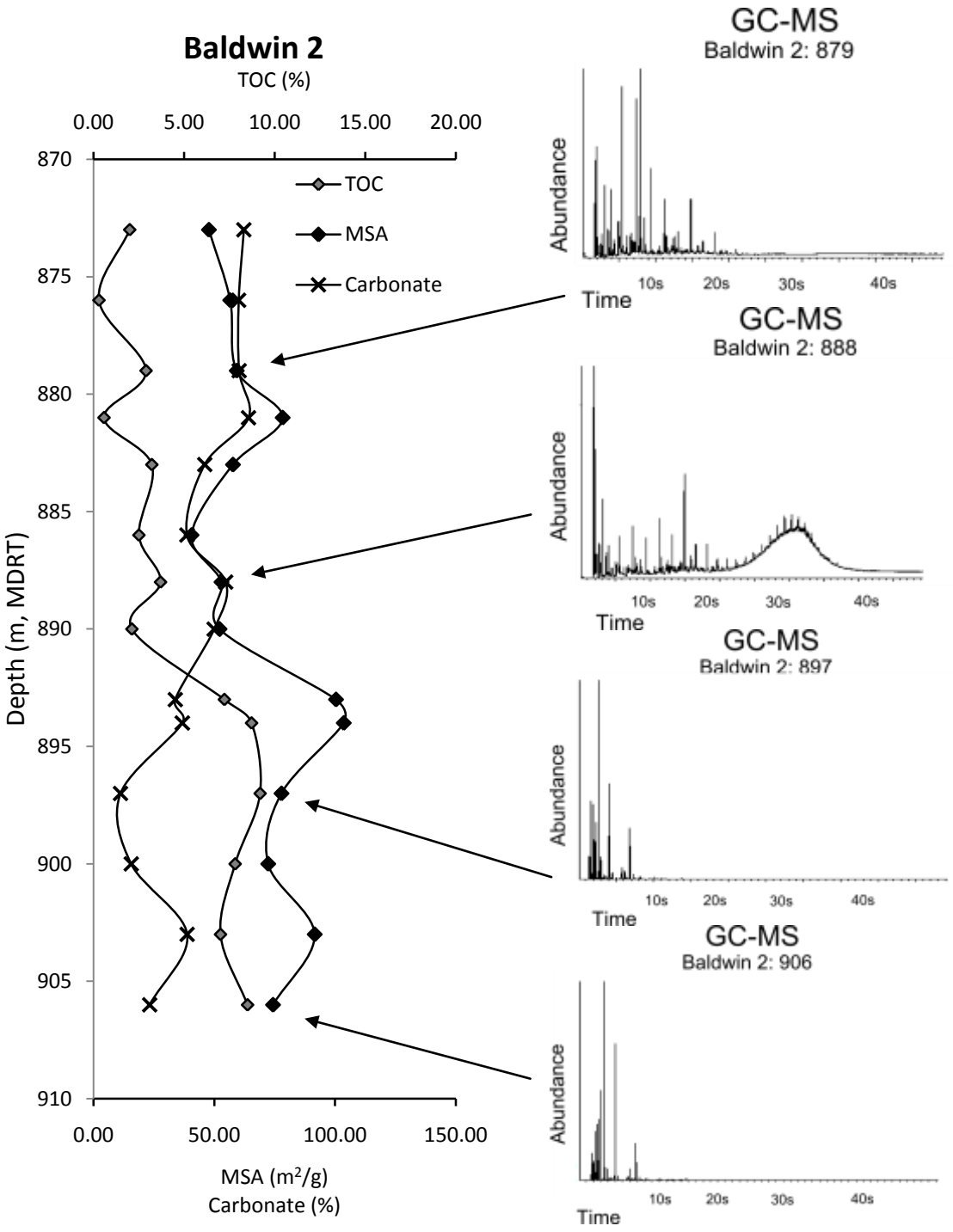

Figure 9: Depth relation between MSA, TOC and Carbonate for Baldwin 2. MSA and TOC values used were corrected for carbonate content through subtraction. GC-MS hydrocarbon profiles are shown adjacent to depth plots. Clay standards we run simultaneously; STx-1b, SWy-2, M.Std, M.Wth, and IMt-2. Standards returned relative standard errors of 1.27%, 0.37%, 2.74%, 2.64% and 6.34% respectively.

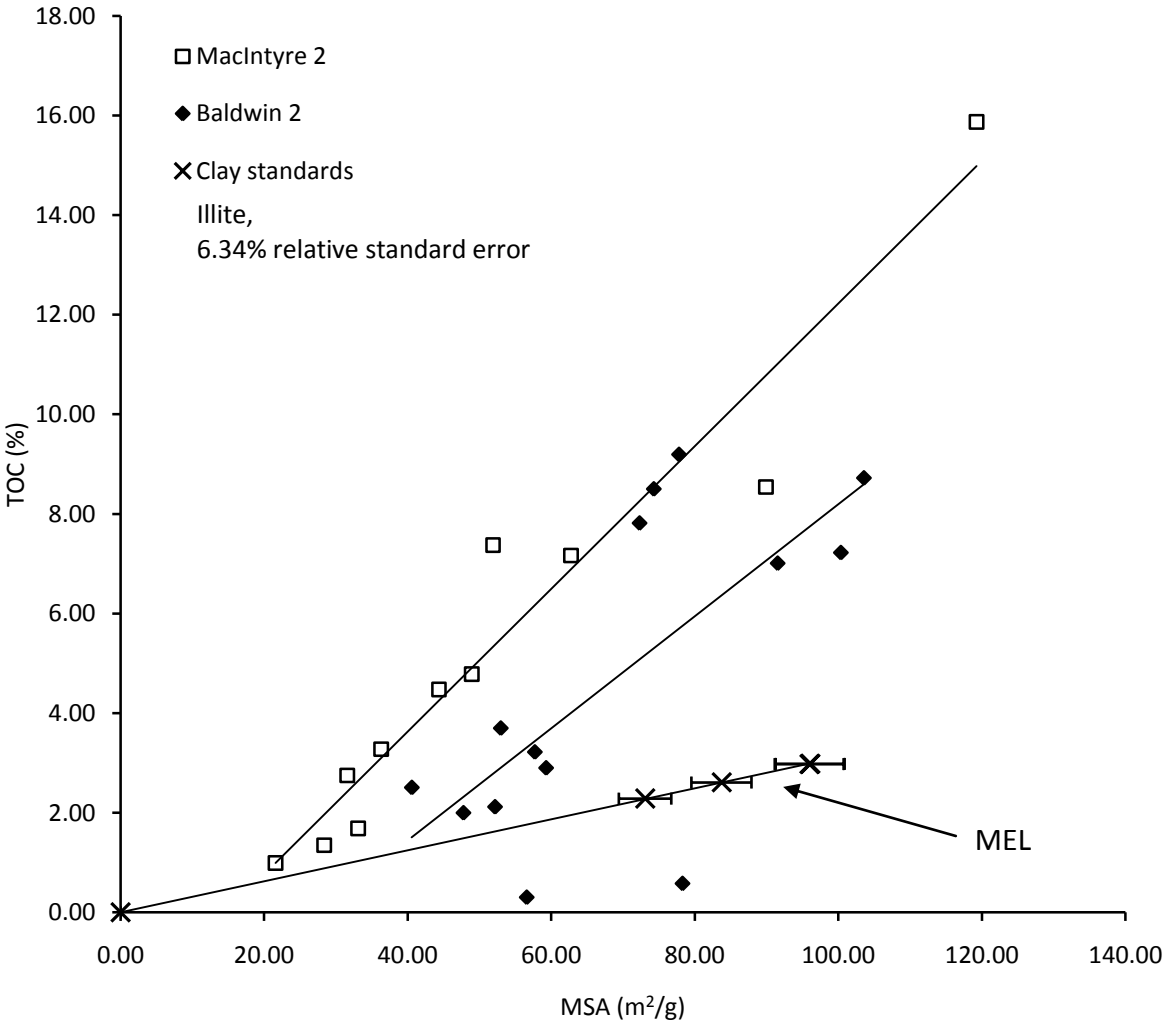

Figure 10: Cross plot of TOC against MSA for MacIntyre 2 and Baldwin 2. MSA and TOC values used were corrected for carbonate content through subtraction. Line equivalent to a monolayer OM coating (MEL) is used here to aid in interpreting the relationship, and was created using illite clay standards (IMt-2, Clay Mineral Society). Relative standard error of illite standards was 6.34%. See Figure 11 for comparative MSA/TOC slope, plotted against thermally immature smectitic samples from Kennedy et al. (2002). Clay standards were run simultaneously; STx-1b, SWy-2, M.Std, M.Wth, and IMt-2. Standards returned relative standard errors of 1.27%, 0.37%, 2.74%, 2.64% and 6.34% respectively.

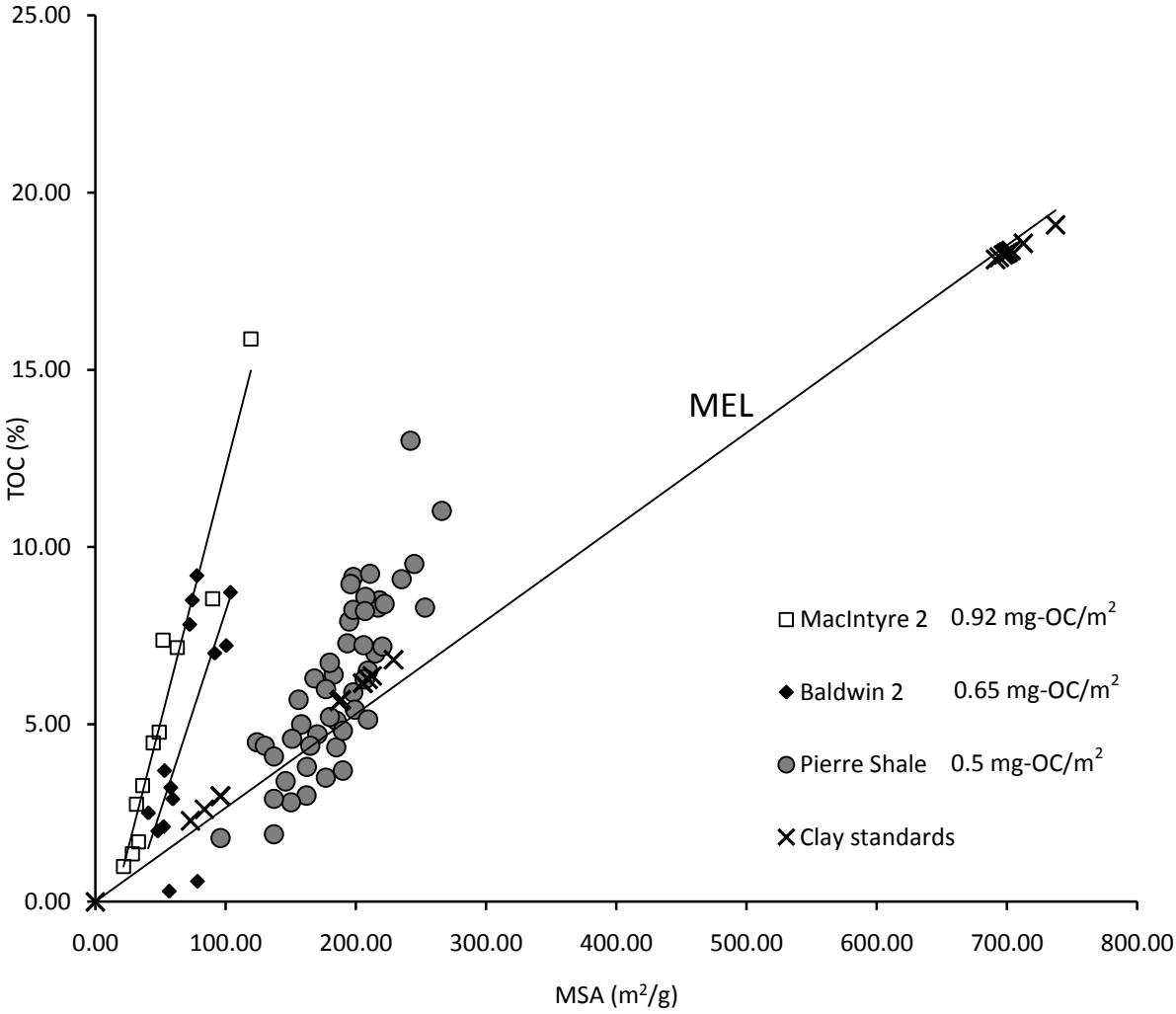

Figure 11: Comparative cross plot of TOC against MSA illustrating difference in loading of organic carbon on mineral surfaces between the thermally mature sediments MacIntyre 2 (0.92 mg-OC/m$^{2)}$ and Baldwin 2 (0.65 mg-OC/m^2) from the current study and thermally immature sediments Pierre Shale (0.5 mg-OC/m^2) from Kennedy et al. (2002) and Kennedy and Wagner (2011). Line equivalent to a monolayer OM coating (MEL) is used here to aid in interpreting the relationship, and was created using illite clay standards (STx-1b, SWy-2, M.Std, M.Wth and IMt-2). Clay standards were run simultaneously; STx-1b, SWy-2, M.Std, M.Wth, and IMt-2. Standards returned relative standard errors of 1.27%, 0.37%, 2.74%, 2.64% and 6.34% respectively.

DISCUSSION

The results of this study show a positive linear relationship between MSA and TOC, as illustrated in Figures 10 & 11. This relationship is consistent with the results of previous studies conducted on continental margin sediments (Mayer 1992; Mayer 1994; Keil *et al.* 1994 A; Ransom *et al.* 1997; Ransom *et al.* 1998; Salmon *et al.* 2000; Kennedy and Wagner 2011). These studies suggested that a first order relation between MSA and OM and was a result of the preservation of OM on mineral surfaces and swelling clays, such as smectite and mixed-layer illite/smectite.

The relationship observed in the current study is characterized by EGME-determined MSA values which fall below previously observed values for sample sets containing thermally immature smectite and mixed layer illite/smectite (Kennedy *et al.* 2002; Kennedy and Wagner 2011) (Figure 11). XRD analysis revealed a relatively consistent mineralogy between samples, and the presence of illitic clays (Table I, Figures 4 & 5). Neither smectite nor mixed-layer illite/smectite was evident (Table II). Interestingly, TOC values calculated in this study are similar to those of the aforementioned studies, despite substantially lower MSA. This observation contrasts the MSA/TOC relationship identified within thermally immature sediments, e.g. Kennedy *et al.* (2002), demonstrating similar loadings of organic carbon in spite of thermal maturation and diminished MSA.

Illite identified within the samples of the current study have two possible origins; detrital and diagenetic. Detrital illite forms through the physical weathering of mica

from igneous and metamorphic rocks (Chamley 1989). Diagenetic illite forms through the illitization of smectite. Illitization involves the expulsion of interlayer ions and H_2O from smectite, replaced by K^+ ions and an associated increase in layer charge as Al^{+3} replaces Si^{+3} in the illite lattice (Chamley 1989; Velde 1992; Pollastro 1993; de Kamp 2008). Illitization occurs during burial and lithification of sediments and requires a source of potassium. Temperatures for illitization roughly coincide with the 'oil-window' ranging from 100˚-110˚C (Pollastro 1993). Illitization causes the collapse of smectite interlayers, reducing the total MSA from $750m^2/g$ to $110m^2/g$.

To understand the observed relationship between MSA and TOC it is necessary to identify whether the illite within the samples is detrital or of diagenetic origin. If the sediments have undergone illitization without any significant loss of OM, then a higher loading of OM per unit surface area should be observed compared to that of the original smectite, which would have significantly more MSA during deposition prior to illitization. If the sediments have experienced a loss of MSA and retention of original OM, it would be apparent as a steeper regression between TOC and MSA (later discusses, Figure 13). This would be consistent with relationships observed in previous studies and show that even after illitization OM is able to retain a proportional relationship with the clay phase established during initial deposition. If however, detrital illite is responsible for the observed relationship, it would imply that OM can be preserved on external mineral surfaces with higher surface loading values than typically observed and on geological timescales. This would be in contrast to studies highlighting the importance of internal surface area of smectitic minerals for OM preservation (Kennedy *et al.* 2002; Williams *et al.* 2005; Kennedy 2011).

To distinguish between detrital and diagenetic illite, samples believed to be representative of the sample set were selected for slow-scan XRD (12s dwell time, 0.02˚, 3.5˚2θ - 50˚2θ). Using response patterns from Moore and Reynolds (1996) as references, the diagnostic peaks of detrital and diagenetic illite were identified in samples M2-870, B2-879 and B2-897 (Figure 7). This suggests that, although physical weathering was responsible for the presence of some illite, smectite was indeed a precursor mineral within the formation and experienced subsequent illitization. Since illitization occurs at temperatures coinciding with the oil-window, the presence of diagenetic illite also suggests that the sediments have entered the oil-window and have likely generated and released hydrocarbons; if migration occurred this would reduce their original TOC values. Gas chromatography-mass spectrometry (GC-MS) hydrocarbon profiles from selected samples (Figures 8 & 9) support this conclusion.

Samples from the current study display organic carbon loading (OC-loading) values noticeably higher than those calculated in previous studies on smectitic shales, e.g. Kennedy *et al.* (2002) and Kennedy & Wagner (2011). Samples herein are characterised by OC-loadings of 0.91mg-OC/m^2 (MacIntyre 2) and 0.65mg-C/m^2 (Baldwin 2), as illustrated in Figure 12. Interestingly, the thermally mature sediments of the current study display OC-loadings almost double that of the thermally immature sediments (Pierre Shale) from Kennedy *et al.* (2002) and Kennedy & Wagner (2011), which averaged 0.5mg-C/m^2 (Figure 11). There is also a notable difference in TOC scaling with MSA between the wells and their respective OC-loadings (Figures 8, 9 & 11).

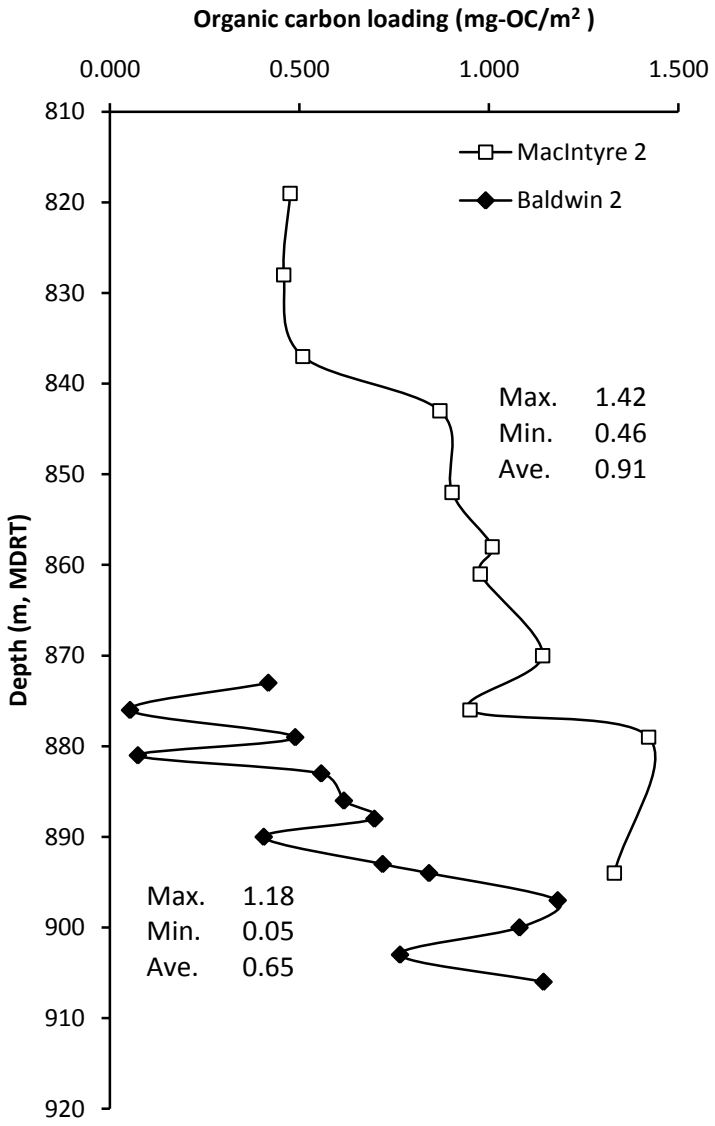

Figure 12: Cross plot of organic carbon loading (OC-loading) against depth for MacIntyre 2 and Baldwin 2. OC-loadings calculated using carbonate corrected TOC and MSA values. For comparison to thermally immature sediments of Kennedy *et al.* (2002) and Kennedy & Wagner (2011) refer to Figure 11.

The presence of illite within samples indicates that the MSA/TOC relationship observed in the current study has one of two origins; either through depositional loading of OM on smectite mineral surfaces, or, through diagenetic alteration caused by MSA loss (illitization) or TOC loss (hydrocarbon generation). A line equivalent to that of a monolayer coating (monolayer equivalent line, MEL) of OM is used here to help interpret the cause of the observed relationship (Figure 13).

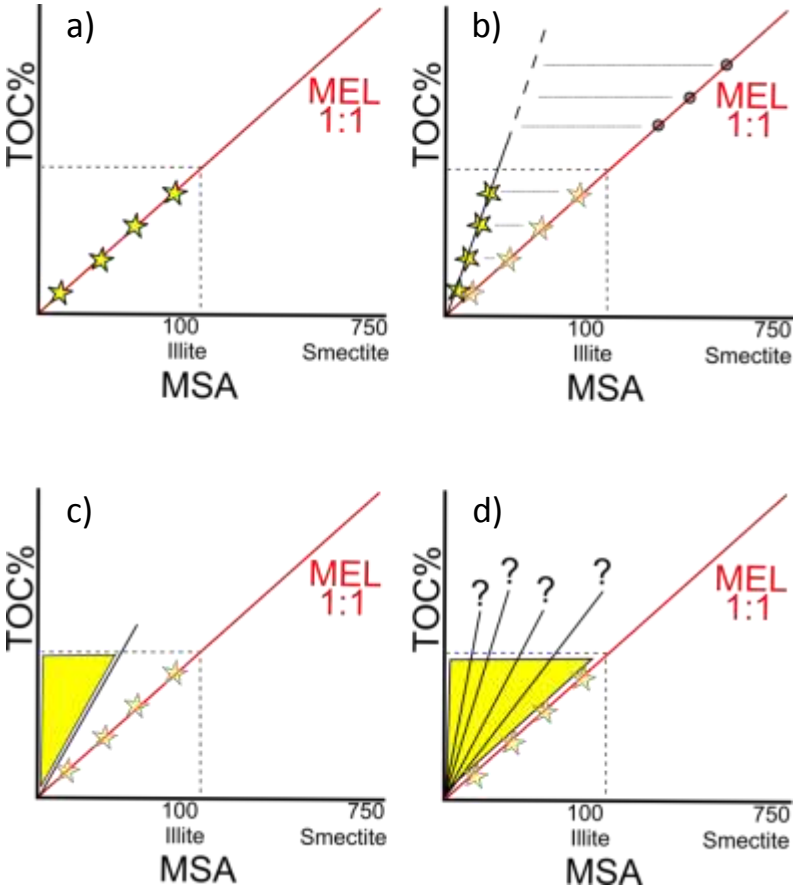

Figure 13: Relationship of MEL to possible MSA/TOC values; a) Depositional relationship, sample TOC scales with MSA on with a 1:1 relationship; b) Diagenetic relationship; MSA loss from illitization without hydrocarbon migration; c) Diagenetic relationship; MSA loss from illitization and hydrocarbon generation or migration; d) Diagenetic relationship; MSA and relative TOC loss from addition of material (e.g. quartz or carbonate cement). MEL is used only as a comparative aid to help interpret origin of MSA/TOC relationship. Solid stars and wedges represent possible data points; faded stars represent data points with idealised OM monolayer coating.

If the samples plot along MEL (Figure 13a) a depositional relationship is interpreted, based on TOC scaling with clay MSA, as seen in studies of immature sediments, e.g. Kennedy *et al* (2002). If a steeper slope is identified whilst retaining a linear correlation it would imply loss of MSA with little or no reduction in TOC, i.e. illitization occurred without generation and migration of hydrocarbons (Figure 13b). Alternatively, both MSA and TOC could be reduced through illitization and migration respectively, causing a sporadic yet clumped data trend steeper than the MEL (Figure 13c). Finally the TOC and MSA could both be reduced by the input of material, i.e. cement, causing samples to plot steeper than the MEL (Figure 13d). The addition of diagenetic cement causes a lower TOC, because it is calculated as a ratio of OC to total sediment mass. By increasing total mass while maintaining constant OC content, the TOC is reduced. Similarly, the reduction in MSA is caused by the cement filling pores. Whilst the effect of carbonate cement has been removed through subtraction; quartz cement is not accounted for and could have a slight reducing effect on MSA and TOC.

The steeper slope of MSA/TOC observed in the current study compared to that of the MEL demonstrates that samples from both wells have an OC-loading greater than that of a monolayer (Figure 8, 13). This suggests the relationship observed in MacIntyre 2 and Baldwin 2 probably resulted from diagenesis, rather than through deposition. Comparisons between wells identifies a narrower MSA spread for MacIntyre 2 compared to Baldwin 2 (Figure 8), suggesting samples from MacIntyre 2 retain a stronger relation between MSA and TOC than those from Baldwin 2, possibly related to the degree of diagenetic alteration. Sediments through the sampled interval of MacIntyre 2 are gas-mature, while those in Baldwin 2 are oil-mature (Figure 1);

implying greater thermal alteration of sediments within MacIntyre 2. The observed variability of the MSA/TOC relationship between wells may thus result from post burial adsorption of migrating hydrocarbons; this possibility is supported by evidence of biodegradation identified in GC-MS data.

GC-MS data acquired over both wells indicates the presence of insitu and migrated hydrocarbons. Migration was inferred from the observation of unresolvable complex masses (UCM), characteristic of degradation and only possible after migration from their source, regardless of migration scale (Peters *et al.* 2005). The degradation observed was interpreted as biodegradation by Boreham and Ambrose (2007) who also conducted GC-MS analysis on Arthur Creek Formation samples. The same study also identified three different petroleum systems corresponding to the Hagen Member (Chabalowe Formation), Arthur Creek Formation and the Thorntonia Limestone. Notably, samples from the current displaying prominent UCM appear to be biodegraded versions of nearby in-situ hydrocarbons, suggestive of only local migration (i.e. within the same petroleum system), and are likely part of the petroleum system within the Arthur Creek Formation. The anomalous hydrocarbon profile identified at the base of MacIntyre 2 is likely from the Thontonia Limestone petroleum system. Interestingly, the occurrence of non-degraded hydrocarbons coincides with the closest MSA/TOC correlations for both wells (Figures 8 & 9). The observed association to non-degraded hydrocarbons suggests that clays may be able to take up hydrocarbons during or after thermal maturation and that MSA may place a control on this association.

The results of this study seem to contrast the standard paradigm of anoxia-dependent OM preservation, whereby OM particles are considered physically independent of the sediments within which they are deposited. MacIntyre 2 samples suggest otherwise through the scaling of TOC with MSA, although noticeably, the same scaling is not as strong within samples from Baldwin 2. Interestingly, comparing GC-MS responses to the MSA/TOC distributions for both MacIntyre 2 and Baldwin 2 (Figure 7) identifies the closest correlations of MSA to TOC occurring where non-degraded hydrocarbons are present. Despite both wells displaying the strongest correlation at the base of the 'Hot Shale' and with the occurrence of non-degraded hydrocarbons (Figure 7), there is a clear difference in scaling of TOC with MSA between the wells, suggestive of either a compositional or diagenetic difference existing between the MacIntyre 2 and Baldwin 2 sediments. The later possibility is supported by evidence of consistent mineralogy (Table I) as well as the steeper MSA/TOC plot compared to the MEL (Figure 8).

Data from the current study appears to suggest that clays are able to take up hydrocarbons within the diagenetic environment during/after hydrocarbon migration, as well as in the depositional setting, as seen through TOC scaling with MSA in thermally immature sediments (Kennedy *et al.* 2002; Kennedy and Wagner 2011). Furthermore, referring back to the MSA/TOC cross-plots (Figures 8 & 9), it appears that as thermal maturity increases so too does the OC-loading of the host sediment. This observation, as well as the scaling of TOC to MSA, suggests OM is in some way controlled by sediment MSA and that thermal maturity, and consequent illitization, enhancing organo-mineral interactions.

In a study conducted on clay mineral transformation in thermally mature gas shales (Metwally and Chesnokov 2012), it was demonstrated using laboratory treated smectite that large quantities of silica are released during illitization, resulting in the formation of quartz cement. The study hypothesized that tight shale formations would act as a locally closed system during diagenesis, and observed through scanning electron microscopy (SEM) that the silica precipitated as granular quartz with intragranular porosity. Perhaps intragranular porosity facilitates encapsulation of hydrocarbons migrated from neighbouring smectitic clays during illitization; this however, is a speculative theory and requires further study.

CONCLUSION

The working hypothesis for this study was that OM concentrations scale with MSA and that without clay minerals present OM is not preserved. The results of this study partially support this hypothesis and suggest the standard paradigm of anoxia driven OM preservation is an inaccurate model. The scaling of TOC to MSA within samples from MacIntyre 2 and partial scaling of those from Baldwin 2 (Figure 7), in conjunction with consistently higher MSA values for Baldwin 2 (Figure 8), illustrates how MSA is a factor controlling OM preservation, in support of the working hypothesis. Interestingly however, higher OC-loadings from the current study compared to smectitic sediments of previous studies demonstrates that MSA may not play as strong as a role as previously thought. MSA/TOC slope comparison to the MEL suggests the relationship observed herein is diagenetic rather than depositional. Despite evidence of illitization, OC-loadings are almost double those from thermally immature sediments, suggesting that perhaps the process of illitization enhances OM preservation. This is partially supported by the observations made by Metwally & Chesnokov (2012) of quartz cement containing intragranular porosity precipitating during illitization; the porosity may provide physical protection of hydrocarbons through encapsulation. Whether this proposed role of illitization is preservative, or, merely as an accumulator or generated hydrocarbon may be an area of future research. Evidence of biodegraded hydrocarbons also suggests the possibility that clay minerals are able to absorb migrating hydrocarbons, becoming associated with organic carbon in the deep burial environment.

ACKNOWLEDGMENTS

First off, I would like to thank Prof. Martin Kennedy for providing me with the opportunity to further my undergraduate study and undertake such an interesting field of research as well as providing constant critical reviews of work. I would like to acknowledge the tremendous ongoing support of Dr. Stefan Löhr and Dr. Phillip Anthony 'Tony' Hall for providing constant critical reviews of work as well as expert technical and analytical assistance. I would also like to acknowledge Samuel Fraser and Claire Thomas for critically reviewing work, as well as Robyn Williamson, Paschal O'Hare, Christopher Kemp and Jesse Castle for providing laboratory assistance. Lastly, I would like to thank PetroFrontier Corp. Pty. Ltd. for graciously providing me with sample and well data.

REFERENCES

Ambrose, G., P. Kruse and P. Putnam (2001). "Geology and hydrocarbon potential of the southern Georgina Basin, Australia." APPEA **41**(Part 1).

Ambrose, G. J. and P. T. Putnam (2005A). "The Georgina Basin." Northern Territory Geological Survey.

Ambrose, G. J. and P. T. Putnam (2005B). "Carbonate ramp facies and oil plays in the Middle–Late Cambrian, southern Georgina
Basin, Australia." PESA.

Bergamashi, B. A., E. Tsamakis, R. G. Keil, T. I. Eglinton, D. B. MontlucËon and J. I. Hedges (1997). "The effect of grain size and surface area on organic matter, lignin and carbohydrate concentration, and molecular composition in Peru Margin sediments." Geochimica et Cosmochimica Acta **61**.

Bohacs, K. M., J. George J. Grabowski, C. Alan R, P. J. Mankiewicz, K. J. Miskell-Gerhardt, J. R. Schalback, M. B. Wegner and J. A. Simo (2005). "Production, Destruction, and Dilution—the Many Paths to Source-Rock Development." Society of Sedimentary geology **Special Publication No. 82**: 61-101.

Boreham, C. J. and G. J. Ambrose (2007). "Cambrian petroleum systems in the southern Georgina Basin, Northern Territory, Australia." Special Publication Northern Territory Geological Survey. Pages: 2.

Bustin, A. M. M., R. M. Bustin, X. Cui and F. A. Inc. (2008). Importance of fabric on the production of gas shales. SPE Unconventional Reservoirs Conference, 10-12 February 2008, Keystone, Colorado, USA, Society of Petroleum Engineers

Chamley, H. (1989). Clay Sedimentology, springer-Verlag Berlin Heidelberg New York.

Cihacek, L. J. and J. M. Bremner (1979). "A Simplified Ethylene Glycol Monoethyl Ether Procedure for Assessment of Soil Surface Area." Soil Science Society of America Journal **43**(4): 821-822.

Coleman, M. L., C. D. Curtis and H. Irwin (1979). "Burial rate a key to source and reservoir potential." World Oil **188**(4): 83-86, 88, 92.

Curry, K. J., R. H. Bennett, L. M. Mayer, A. Curry, M. Abril, P. M. Biesiot and M. H. Hulbert (2007). "Direct visualization of clay microfabric signatures driving organic matter preservation in fine-grained sediment." Geochimica Et Cosmochimica Acta **71**(7): 1709-1720.

de Kamp, P. C. v. (2008). "Smectite-illite-muscovite transformations, quartz dissolution, and silica release in shales." Clays and Clay Minerals **56**(1): 66-81.

Demaison, G. J. and G. T. Moore (1980). "Anoxic environments and oil source bed genesis." Organic Geochemistry **2**(1): 9-31.

Dunster, J., P. Kruse, M. Duffett and G. Ambrose (2007). "Geology and resource potential of the southern Georgina Basin." Northern Territory Geological Survey.

Hall, A., D. M. McKirdy, G. P. Halverson, J. B. Jago and J. G. Gehling (2011). "Biomarker and isotopic signatures of an early Cambrian Lagerstätte in the Stansbury Basin, South Australia." Organic Geochemistry **42**(11): 1324-1330.

Hall, P. A., A. F. R. Watson, G. V. Garner, K. Hall, S. Smith, D. Waterman and B. Horsfield (1999). "An investigation of micro-scale sealed vessel thermal extraction-gas chromatography-mass spectrometry (MSSV-GC-MS#) and micro-scale sealed vessel pyrolysis-gas chromatography-mass spectrometry applied to a standard reference material of an urban dust/organics." Science of The Total Environment **235**(1–3): 269-276.

Hedges, J. I. and R. G. Keil (1995). "Sedimentary organic matter preservation: an assessment and speculative synthesis." Marine Chemistry **49**(2-3): 81-115.

Hill, A. C. and M. R. Walter (2000). "Mid-Neoproterozoic (~830–750 Ma) isotope stratigraphy of Australia and global correlation." Precambrian Research **100**(1–3): 181-211.

Jing, W., L. Huiqing, G. Rongna, K. Aihong and Z. Mi (2011). "A New Technology for the Exploration of Shale Gas Reservoirs." Petroleum Science and Technology **29**(23): 2450-2459.

Katz, B. (2005). "Controlling factors on source rock developments - a review or productivity, preservation, and sedimentation rate." The Deposition of Organic-Carbon-Rich Sediments: Models, Mechanisms, and Consequences **Special Publication No. 82**: 7-16.

Keil, R. G. and J. I. Hedges (1993). "Sorption of organic matter to mineral surfaces and the preservation of organic matter in coastal marine sediments." Chemical Geology **107**(3-4): 385-388.

Keil, R. G., D. B. Montlucon, F. G. Prahl and J. I. Hedges (1994 B). "Sorptive preservation of labile organic matter in marine sediments." Nature **370**(6490): 549-552.

Keil, R. G., E. Tsamakis, C. B. Fuh, J. C. Giddings and J. I. Hedges (1994 A). "Mineralogical and textural controls on the organic composition of coastal marine sediments: Hydrodynamic separation using SPLITT-fractionation." Geochimica Et Cosmochimica Acta **58**(2): 879-893.

Kennedy, M. J. (2011). "From Organo-mineral Nanocomposite to Australian Basins; an Intergrated Approach to Unconventional Gas Exploration and Development." funding proposal.

Kennedy, M. J., D. R. Pevear and R. J. Hill (2002). "Mineral surface control of organic carbon in black shale." Science **295**(5555): 657-660.

Kennedy, M. J. and T. Wagner (2011). "Clay mineral continental amplifier for marine carbon sequestration in a greenhouse ocean." Proceedings of the National Academy of Sciences of the United States of America **108**(24): 9776-9781.

Lindsay, J. F. (2002). "Supersequences, superbasins, supercontinents - evidence from the Neoproterozoic-Early Palaeozoic basins of central Australia." Basin Research **14**(2): 207-223.

Lunsdorf, H., R. W. Erb, W. R. Abraham and K. N. Timmis (2000). "'Clay hutches': a novel interaction between bacteria and clay minerals." Environmental Microbiology **2**(2): 161-168.

Mayer, L. M. (1992). "Adsorption into mineral mesopores as a stabilization mechanism for organic matter on aluminosilicates." Abstracts with Programs Geological Society of America **24**(7): 22.

Mayer, L. M. (1994). "Surface-Area Control of Organic-Carbon Accumulation in Continental-Shelf Sediments." Geochimica Et Cosmochimica Acta **58**(4): 1271-1284.

Mayer, L. M., P. T. Rahaim, W. Guerin, S. A. Macko, L. Watling and F. E. Anderson (1985). "Biological and granulometric controls on sedimentary organic matter of an intertidal mudfat." Estuarine Marine and Coastal Shelf Science **20**.

Metwally, Y. M. and E. M. Chesnokov (2012). "Clay mineral transformation as a major source for authigenic quartz in thermo-mature gas shale." Applied Clay Science **55**(0): 138-150.

Moore, D. M. and R. C. Reynolds (1996). "X-Ray Diffraction and the identification and Analysis of Clay Minerals. Second Edition.".

Pegum, D. M. (1997). "An introduction to the petroleum geology of the Northern Territroy of Australia." Department of Mines and Energy, Northern Territory geological survey.

Peters, K. E., C. C. Walters and J. M. Moldowan (2005). The Biomarker Guide, Volume 2: Biomarkers and Isotopes in the Petroleum Exploration and Earth History Cambridge University Press.

Pollastro, R. M. (1993). "Considerations and applications of the illite/smectite geothermometer in hydrocarbon-bearing rocks of Miocene to Mississippian age." Clays and Clay Minerals **41**(2): 119-133.

Ransom, B., R. H. Bennett, R. Baerwald and K. Shea (1997). "TEM study of in situ organic matter on continental margins: occurrence and the "monolayer" hypothesis." Marine Geology **138**(1–2): 1-9.

Ransom, B., D. Kim, M. Kastner and S. Wainwright (1998). "Organic matter preservation on continental slopes: importance of mineralogy and surface area." Geochimica Et Cosmochimica Acta **62**(8): 1329-1345.

Salmon, V., S. Derenne, E. Lallier-Vergès, C. Largeau and B. Beaudoin (2000). "Protection of organic matter by mineral matrix in a Cenomanian black shale." Organic Geochemistry **31**(5): 463-474.

Schuchert, C. (1915). "The Conditions of Black Shale Deposition as Illustrated by the Kupferschiefer and Lias of Germany." Proceedings of the American Philosophical Society **54**(218): 259-269.

Shaw, D. B. and C. E. Weaver (1965). "The mineralogical composition of shales." Journal of Sedimentary Research **35**(1): 213-222.

Shergold, J. H. and H. B. Whittington (2000). "The Cambrian trilobite Bathynotus (?Redlichioidea) in the Northern Territory, Australia." Alcheringa: An Australasian Journal of Palaeontology **24**(1): 1-10.

Sherrod, L. A., G. Dunn, G. A. Peterson and R. L. Kolberg (2002). "Inorganic carbon analysis by modified pressure-calcimeter method." Soil Science Society of America Journal **66**(1): 299-305.

Smith, K. (1972). "Stratigraphy of the Georgina Basin." Department of national development - bureau of mineral resources, geology and geophysics **Bulletin No. 111**.

Suess, E. (1973). "Interaction of organic compounds with calcium carbonate, II. Organo-carbonate associations in recent sediments." Geochimica et Cosmochimica Acta **37**.

Tanoue, E. and N. Handa (1979). "Differential sorption of organic matter by various sized sediments particles in Recent sediment from the Bering Sea." Journal of the Oceanographic Society of Japan **35**.

Tiller, K. and L. Smith (1990). "Limitations of EGME retention to estimate the surface area of soils." Soil Research **28**(1): 1-26.

Tyson, R. V. (2001). "Sedimentation rate, dilution, preservation and total organic carbon: some results of a modelling study." Organic Geochemistry **32**(2): 333-339.

U. S. Geological Survey (2011). "A Laboratory Manual for X-Ray Powder Diffraction."

Velde, B. (1992). Introduction to clay minerals. Chemistry, origins, uses and environmental significance., Chapman & Hall.

Williams, L. B., B. Canfield, K. M. Voglesonger and J. R. Holloway (2005). "Organic molecules formed in a "primordial womb"." Geology **33**(11): 913-916.

Appendix A

Extended methodology

Initial sample preparation:

Dry all samples overnight in 40˚C oven.

Grind all samples and pass through 0.0097" sieve.

Store all samples in 40˚C oven until use.

Mineral Surface Area (MSA) – EGME:

Sample preparation for EGME

1. Weigh out 1.1g of sample into 50mL centrifuge tube.
2. Pour 15mL of Calcium Chloride ($CaCl_2$) solution (1 M) into each centrifuge tube and shake vigorously for approximately 30seconds, followed by 1hr in an end-over-end rotator.
3. Place sample-filled centrifuge tubes into centrifuge and run at 3000rpm for 15mins.
4. If samples have not consolidated at the base of the test tube, centrifuge for a further 15mins, continue as required.
5. If the samples continue to remain unconsolidated, consider a higher speed or filtering of the solids from the liquid.
6. Leave samples to rest for 1hr, then fill up to 50mL with de-ionised (DI) water and run samples through centrifuge at 3000rpm for 15mins.
7. Pour out supernatant, being careful not lose any sample.
8. Fill tubes with 45mL of DI water, shake vigorously, and run samples through centrifuge at 3000rpm for 15mins. Pour out supernatant.
9. Repeat Step 7. & Step. 8 once more.
10. Remove lids and place centrifuge tubes in 40˚C oven until dry.

Once are samples have been dried in 40˚C oven for at least 48hrs, they can be re-ground ready for MSA determination.

1. Label all glass vials and lids with respective sample numbers using diamond tipped scribe.
2. Weigh the glass vials and lids. Measure to as many significant digits as possible (e.g. 4-5 decimal places).
3. Place 1g of sample (post $CaCl_2$ exchange) into each respective vial and allow to dry (uncapped) in 110˚C oven for 48hrs.
4. Remove vials from oven and cap immediately, place in desiccator to cool for 1hr, or until at room temperature.
5. When cool, record the total weight of the capped vials; sample + vial + lid. Calculate the sample weight.
6. Underneath a fume hood, place 1mL of 1M solution of EGME into each vial.
7. Place all (uncapped) vials into the vacuum chamber. Make sure to note the position of each vial relative to its lid (outside the chamber) for ease of capping upon removal. It is important to minimise the sample/EGME mixture's atmospheric contact as much as possible.
8. Place beaker with approximately 40mL of EGME and a petri dish with approximately 200g of $CaCl_2$ granules at the base of the vacuum chamber.
9. Close and lock pressure chamber. Evacuate the chamber by running the vacuum pump for 5mins, at least 85psi. Make sure to close the valve when the pump is off.
10. Leave the samples in the vacuum chamber for 2weeks, replacing the EGME and $CaCl_2$ granules as needed (about every 2days). When opening the vacuum

chamber make sure to slowly release the pressure beforehand, otherwise the sudden pressure change will blow the vials over. Re-evacuate chamber each time chamber is opened.

11. After 2 weeks have passed, record the total weight of the vials (lid on) every 2days until their weight has stabilized. It is very important to cap the vials as soon as possible when removing from the vacuum chamber. Replace EGME and $CaCl_2$ as required.

Carbonate pressure test – TOC Part 1

This step is to measure the total amount of calcium carbonate within the sample. This is used in conjunction with the total carbon results to determine the total organic carbon content (TOC %) of the sample.

1. Cut 2mL micro-centrifuge test tubes such that they hold exactly 1mL of liquid.
2. Fill all (approx. 20mL) glass vials with 5mL of HCl, leave to one side.
3. Weigh 200mg of sample into cut micro-centrifuge tubes and place the filled tube into the HCl using tweezers. Ensure that the sample does not come into contact with the HCl.
4. Place rubber seal on vial and crimp metal cap onto vial, making sure not to allow the sample and HCl to mix.
5. Repeat Step. 6 for all samples.
6. Include 7 $CaCO_3$ standards at 200mg, 150mg, 100mg, 75mg, 50mg, 20mg and 10mg
7. Shake all vials vigorously for 1min and leave to stand for 1hr. Make sure that the entirety of the samples have mixed with the HCl, re-shake after 30mins.
8. Use manometer and needle to measure pressure within each vial. Ensure that the puncturing needle does not move once in the vial, or pressure will be released.
9. Create a calibration curve using the standard $CaCO_3$ results.
10. Based on the trend line equation for $CaCO_2$ standards, calculate the $CaCO_3$ % within each sample, and then convert this into inorganic carbon content by multiplying by 0.12.

Total carbon analysis, LECO CHN, - (TOC Part 2)

This method should be followed when running standards and unknown samples. Prior to running unknown samples it is imperative to run standards. Procedure on following page.

1. Measure 200mg of unknown sample/standard sample into tin foil 'bowl'.
2. Wrap the tin foil 'bowl' into small tube, approx. 10mm x 5mm
3. Place sample into the next auto-sampler and run LECO.
4. After each analysis check the auto-sampler to ensure that the sample has dropped into the machine.

Prior to running unknown samples

1. Run 5 'blanks' (empty tin foils) then select the 3 with the most consistent results and perform a 'blank correction' on these 3.
2. Run 2 EDTA standards (stds) of 100mg. The results for these stds should fall within the margin of error, as indicated on sample container.
3. If EDTA stds are acceptable then perform a 'drift correction'.
4. Run 2 each of $CaCO_3$ and Quartz (Qtz) at 200mg, if within margin of error then continue with samples; $CaCO_3$ = 11.9 +/- 0.2% & Qtz = 0% +/- 0.2%

Running unknown samples

1. If stds are ok, then begin running unknown samples at 200mg. Between each sample make sure that it has loaded correctly into the chamber.
2. Every 10 (or 5) samples run 1 $CaCO_3$ and 1 Qtz, std, each at 200mg.
3. Replace the crucible within the LECO every 20 samples.

X-Ray Diffraction (XRD) – Bulk

1. Insert bulk XRD disc into side-loader.
2. Load approximately 1g of ground sample into disc using spatula up to the fill point of the side-loader. Tap firmly on side to ensure the entirety of the disc is uniformly filled with sample.
3. When filled and no cracks are present, turn the side-loader on its side such that the disc is facing sample-side upwards. Remove the disc from the side-loader, making sure not to slide the disc in any direction; which will result cause the sample to be preferentially orientated. An easy way to ensure randomized particle orientation is to pull the side-loader up away from the disc rather that across the sample.
4. Wipe the edges of the disc clean using a Kim-Wipe, and then gently blow away any excess grains which may have fallen onto the surface of the sample from the loader. Ensure the sample within the disc is perfectly flat, and free from fractures.
5. Run the samples in the XRD (for this experiment a Bruker D8 Advance XRD was used with a Cu source). Scan the samples between 3.5˚2θ - 50˚2θ, with a step size of 0.02˚ and dwell time of 1second.

X-Ray Diffraction (XRD) – Clay separated

1. Cut silicon wafers into equal sized squares such that they fit perfectly within the clay fraction XRD discs.
2. Place approximately 20mg of ground sample into labelled centrifuge tubes and fill with 15mL of DI water.
3. Cap and shake vigorously for 10seconds. To disperse the clay particles throughout the solution place tubes in sonic cleaner partially filled with DI water and run for 5mins.
4. Shake each sample vigorously for 45s and stand for 5mins.
5. Using a new pipette for each sample, remove approximately 0.5mL of solution from the very top of the centrifuge tube and place a few drops onto the silicon wafer; enough to completely cover the slide.
6. Allow the wet silicon wafers to air-dry; alternatively they can be placed within a 40˚C to speed the process.
7. When completely dry place the wafers into XRD discs and run in XRD as per bulk XRD settings.
8. After analysing without EG, place one drop onto the wafer, wait for 10mins then repeat Step. 7.
9. If necessary, refer to a 'clay mineralogical identification flow diagram' and select all samples which show response peaks of interest. For this experiment peaks at 14Å (angstroms) were chosen.
10. Using fresh sample (following Steps. 3-6) re-run the new wafers as per Step. 7.
11. Once run, bake the wafers (not the XRD discs) in a furnace at 400˚C for at least 30minutes, allow to cool and then re-run in the XRD as per Step. 7.

12. Once run, bake the wafers (not the XRD discs) in a furnace at 550˚C for at least 30minutes, allow to cool and then re-run in the XRD as per Step. 7.

Note, for the purposes of this experiment it was not necessary to continue analysis after heating to 550˚C. Any further analysis would not provide additional information.

Gas chromatography-mass spectrometry (GC-MS)

1. Place approximately 10mg of powdered sample into pre-cleaned micr-scale sealed vessel (MSSV) glass reactor tube. Tubes are made of high purity silica, are sealed at one end and have an internal diameter of 100µm with a 120˚ bend in the centre.
2. Fill the 'dead volume' of the tube with pre-cleaned glass beads (80-120 mesh) and seal the tube using a high temperature propane torch.
3. Insert the reactor tube into the injector head (heated at 300˚C) and run through GC cleaning cycle by heating from 45˚-300˚C at 15˚C/min, then hold at 300˚C for 15mins to remove any exterior contaminants from the tube. Note, this cleaning cycle also serves as the thermal desorption stage for non-pyrolysed samples including additional dwell time to extend total run time per sample to 1hr.
4. Crack reactor tubes within the injector and operate in splitless mode for 2mins, with the released analytes cryofocused in the front of the capillary column using a liquid nitrogen bath.

- For this study a Quantum MSSV injector fitted to a Hewlett Packard 6890/5973 GC-MS system was used. A HP5-MS capillary column of 25m length, 0.25mm ID and 0.25µdf coating was used for the separations with helium carrier gas at constant 60KPa pressure.
- GC-MS analysis was conducted in full scan mode, employing a temperature program of 45º-300ºC at 8ºC/min then held isothermal for 17mins. Full scan data were acquired over range of 45-450 amu at approximately 3 scans per sec.

Appendix B

Raw inorganic carbon, total carbon, and total organic carbon data

Sample #	Vial #	Sample mass (mg)	Pressure (mbar)	CaCO3 (%)	Inorganic carbon mass (mg)	Inorganic carbon (%)
*CaCO3	S1	199.49	1355	99.8322	23.8986	11.98
*CaCO3	S2	150.31	1021	99.6540	17.9748	11.96
*CaCO3	S3	99.59	689	101.1351	12.0864	12.14
*CaCO3	S4	74.58	516	100.7656	9.0181	12.09
*CaCO3	S5	51.21	355	100.2835	6.1626	12.03
*CaCO3	S6	20.66	138	93.3330	2.3139	11.20
*CaCO3	S7	10.20	79	103.5529	1.2675	12.43
B2.873	1	201.65	856	62.1884	15.0484	7.46
B2.876	2	201.63	827	60.0688	14.5340	7.21
B2.879	3	201.54	829	60.2423	14.5695	7.23
B2.881	4	200.18	876	64.1218	15.4031	7.69
B2.883	5	201.18	633	45.9507	11.0932	5.51
B2.886	6	200.55	532	38.6516	9.3019	4.64
B2.888	7	200.01	748	54.7176	13.1329	6.57
B2.890	8	201.44	688	49.9268	12.0687	5.99
B2.893	9	200.57	466	33.7842	8.1313	4.05
B2.894	10	200.26	505	36.7149	8.8230	4.41
B2.897	11	201.08	159	11.1331	2.6864	1.34
B2.900	12	201.16	219	15.5371	3.7505	1.86
B2.903	13	200.22	532	38.7153	9.3019	4.65
B2.906	14	200.49	322	23.1821	5.5773	2.78
M2.819	15	200.28	772	56.4149	13.5585	6.77
M2.828	16	200.75	487	35.3000	8.5038	4.24
M2.837	17	201.26	516	37.3403	9.0181	4.48
M2.843	18	200.98	706	51.3648	12.3880	6.16
M2.852	19	200.92	584	42.4056	10.2242	5.09
M2.858	20	200.18	741	54.1543	13.0087	6.50
M2.861	21	200.03	626	45.6976	10.9691	5.48
M2.870	22	200.41	734	53.5759	12.8846	6.43
M2.876	23	200.96	1215	88.8053	21.4156	10.66
M2.879	24	200.07	1074	78.7841	18.9148	9.45
M2.894	25	200.36	1289	94.5300	22.7280	11.34

* standard

Raw inorganic carbon content data, determined through the carbonate-acid pressure test of Sherrod *et al.* (2002). Carbonate content of samples was calculated based on the linear equation created by plotting mass against pressure for known carbonate standards.

Sample #	Total Mass (g)	Nitrogen (mg)	Carbon (mg)	Hydrogen (mg)	Nitrogen (%)	Carbon (%)	Hydrogen (%)
*Blank	1.000	0.492	0.202	-0.038	0.049	0.020	-0.004
*Blank	1.000	0.495	0.203	-0.044	0.050	0.020	-0.004
*EDTA	0.101	10.311	41.701	5.564	10.168	41.125	5.487
*EDTA	0.103	10.445	42.473	5.792	10.101	41.076	5.601
*CaCO3	0.206	0.646	24.676	-0.096	0.313	11.955	-0.046
*CaCO3	0.203	0.547	24.128	-0.026	0.269	11.886	-0.013
*Quartz	0.202	0.560	0.248	-0.032	0.277	0.123	-0.016
*Quartz	0.202	0.502	0.261	-0.039	0.248	0.129	-0.019
B2.873	0.201	0.545	16.517	0.127	0.271	8.218	0.063
B2.876	0.201	0.545	14.722	0.172	0.271	7.328	0.085
B2.879	0.201	0.585	16.864	0.174	0.291	8.382	0.087
B2.881	0.201	0.578	15.851	0.231	0.288	7.902	0.115
B2.883	0.202	0.586	14.660	0.297	0.290	7.254	0.147
B2.886	0.200	0.567	12.363	0.223	0.283	6.175	0.111
B2.888	0.200	0.556	16.464	0.183	0.278	8.240	0.091
B2.890	0.201	0.571	14.194	0.281	0.283	7.051	0.139
B2.893	0.201	0.871	17.727	0.685	0.434	8.837	0.341
B2.894	0.200	0.817	19.893	0.659	0.408	9.927	0.329
B2.897	0.201	0.898	19.072	0.860	0.448	9.508	0.429
*Blank	1.000	1.326	0.192	-0.386	0.133	0.019	-0.039
*Blank	1.000	1.008	0.209	-0.053	0.101	0.021	-0.005
*Blank	1.000	0.596	0.198	-0.061	0.060	0.020	-0.006
*Blank	1.000	0.490	0.199	-0.069	0.049	0.020	-0.007
*Blank	1.000	0.440	0.199	-0.065	0.044	0.020	-0.006
*EDTA	0.100	9.569	41.113	5.563	9.550	41.031	5.552
*EDTA	0.101	9.670	41.617	5.577	9.564	41.164	5.517
*CaCO3	0.202	0.344	24.029	-0.090	0.171	11.925	-0.045
*CaCO3	0.201	0.316	23.914	-0.022	0.157	11.915	-0.011
*Quartz	0.200	0.347	0.282	-0.041	0.173	0.141	-0.021
B2.900	0.200	0.751	16.934	0.720	0.375	8.467	0.360
B2.903	0.201	0.680	18.009	0.680	0.338	8.942	0.338
B2.906	0.201	0.668	18.729	0.699	0.332	9.313	0.348
M2.819	0.202	0.345	14.826	0.198	0.171	7.358	0.098
M2.828	0.201	0.320	9.787	0.310	0.159	4.877	0.155
*CaCO3	0.201	0.288	23.779	-0.027	0.143	11.836	-0.013
M2.837	0.200	0.397	11.063	0.355	0.199	5.537	0.178
M2.843	0.201	0.373	15.040	0.280	0.186	7.501	0.140
M2.852	0.200	0.463	13.966	0.420	0.231	6.976	0.210
M2.858	0.200	0.395	17.101	0.348	0.198	8.551	0.174
M2.861	0.200	0.482	16.187	0.498	0.241	8.081	0.249
*CaCO3	0.201	0.215	23.786	-0.042	0.107	11.851	-0.021
M2.870	0.200	0.392	19.531	0.474	0.196	9.756	0.237

* standard

Raw total carbon content data, as determined using LECO TruSpec CHN (carbon-hydrogen-nitrogen analyser).

End of document.